Journal of Controlled Release 363 (2023) 275–289

Contents lists available at ScienceDirect

Journal of Controlled Release

journal homepage: www.elsevier.com/locate/jconrel

Exosome delivery to the testes for *dmrt1* suppression: A powerful tool for sex-determining gene studies

Tengfei Zhu [a,b], Ming Kong [c], Yingying Yu [d], Manfred Schartl [e,f], Deborah Mary Power [g], Chen Li [a,h], Wenxiu Ma [a,b], Yanxu Sun [a,b], Shuo Li [a,b], Bowen Yue [a,b], Weijing Li [a,b], Changwei Shao [a,b,*]

[a] National Key Laboratory of Mariculture Biobreeding and Sustainable Goods, Yellow Sea Fisheries Research Institute, Chinese Academy of Fishery Sciences, Nanjing Road 106, Qingdao 266071, China
[b] Laboratory for Marine Fisheries Science and Food Production Processes, Qingdao National Laboratory for Marine Science and Technology, Wenhaizhong Road 168, Qingdao 266237, China
[c] College of Marine Life Science, Ocean University of China, Yushan Road 5, Qingdao 266003, China
[d] Guangdong Provincial Key Laboratory of Animal Molecular Design and Precise Breeding, School of Life Science and Engineering, Foshan University, Guangyun Road 33, Foshan 528225, China
[e] Developmental Biochemistry, Biocenter, University of Würzburg, Sanderring 2, Würzburg 97074, Germany
[f] The Xiphophorus Genetic Stock Center, Department of Chemistry and Biochemistry, Texas State University, 601 University Drive, San Marcos, TX 78666, USA
[g] Comparative Endocrinology and Integrative Biology, Centre of Marine Sciences, Universidade do Algarve, Campus de Gambelas, Algarve, Faro 8005-139, Portugal
[h] Key Laboratory of Maricultural Organism Disease Control, Ministry of Agriculture and Rural Affair, Qingdao Key Laboratory of Mariculture Epidemiology and Biosecurity, Yellow Sea Fisheries Research Institute, Chinese Academy of Fishery Sciences, Nanjing Road 106, Qingdao 266072, China

ARTICLE INFO

Keywords:
Engineered exosome
Delivery system
Tissue targeting
dmrt1
Sex-determining gene
microRNA

ABSTRACT

Exosomes are endosome-derived extracellular vesicles about 100 nm in diameter. They are emerging as promising delivery platforms due to their advantages in biocompatibility and engineerability. However, research into and applications for engineered exosomes are still limited to a few areas of medicine in mammals. Here, we expanded the scope of their applications to sex-determining gene studies in early vertebrates. An integrated strategy for constructing the exosome-based delivery system was developed for efficient regulation of *dmrt1*, which is one of the most widely used sex-determining genes in metazoans. By combining classical methods in molecular biology and the latest technology in bioinformatics, isomiR-124a was identified as a *dmrt1* inhibitor and was loaded into exosomes and a testis-targeting peptide was used to modify exosomal surface for efficient delivery. Results showed that isomiR-124a was efficiently delivered to the testes by engineered exosomes and revealed that *dmrt1* played important roles in maintaining the regular structure and function of testis in juvenile fish. This is the first *de novo* development of an exosome-based delivery system applied in the study of sex-determining gene, which indicates an attractive prospect for the future applications of engineered exosomes in exploring more extensive biological conundrums.

1. Introduction

Exosomes, a subtype of extracellular vesicles (EVs) of endosomal origin with diameters from ~50 to 150 nm, have been increasingly focused on by researchers in the past decades because of their involvement in cell-cell communication and therapeutic and diagnostic potential [1]. In addition to their applications as biomarkers for various diseases [2,3], exosomes have great advantages as endogenous nanocarriers owing to their stability, low cytotoxicity, and immunogenicity [4,5]. Furthermore, modifiability of the exosomal surface endows exosomes with high application potential for tissue-targeting delivery of biocargo across biological barriers [6–8]. To date, applications of the engineered exosomes have attracted strong research interests mainly in the field of pharmacology for cancer and neurological diseases in mammals [9]. However, their applications in different species for functional gene studies are still worth exploring in depth to tackle more

* Corresponding author at: National Key Laboratory of Mariculture Biobreeding and Sustainable Goods, Yellow Sea Fisheries Research Institute, Chinese Academy of Fishery Sciences, Nanjing Road 106, Qingdao 266071, China.
E-mail address: shaocw@ysfri.ac.cn (C. Shao).

https://doi.org/10.1016/j.jconrel.2023.09.027
Received 4 April 2023; Received in revised form 13 September 2023; Accepted 14 September 2023
Available online 28 September 2023

extensive biological problems in genetics and evolution.

Sex determination (SD) is the biological process that establishes the testis or ovary developing from the bipotential gonad primordium to provide a microenvironment for sperm or ova generation in sexual reproduction [10]. In some animals, there is a master SD gene acting as the initiating signal at the top of the SD regulatory network, which in turn triggers the genes in the gonadal development pathway. Doublesex and mab-3 related transcription factor 1 (dmrt1) belongs to the family of DM domain genes that play central and conserved roles in sexual differentiation and development across a wide range of animals, and may arise with the emergence of the metazoans [11]. Many studies have showed that dmrt1 controls the SD in fish, frogs, and birds [12–16]. In contrast, dmrt1 is not required for SD in the mouse but is involved in mouse spermatogenesis and maintenance of the testis [17,18]. However, research on the postnatal and post-SD roles of *dmrt1* outside mammals remains insufficient. Therefore, investigations on dmrt1 mutant animals, particularly in early vertebrates, will be informative to understand its possible ancestral roles in evolution.

The Chinese tongue sole (*Cynoglossus semilaevis*) is a flatfish with a female heterogametic (ZW/ZZ) mode of SD. High temperature at larval stage leads to female-to-male sex reversal [19]. Previous studies in our laboratory revealed that dmrt1 was involved in the sex reversal induced by high temperature [20]. Furthermore, female development after *dmrt1* ablation in embryos confirmed that *dmrt1* is the master male SD gene in Chinese tongue sole [21]. Therefore, Chinese tongue sole is a good model to study the postnatal role of dmrt1. To this end, we developed an exosome-based delivery system using both classical experimental methods and the latest bioinformatic approaches. The engineered exosomes were constructed by loading with the newly found miRNA inhibiting *dmrt1* expression and modifying with the first identified peptide for the testis-targeting effect. Applications of the engineered exosomes *in vivo* confirmed that the present exosome-based delivery system was efficient in targeting testes and inhibiting the expression of *dmrt1*. The functional study revealed that *dmrt1* was necessary to maintain the normal structure and regular spermatogenesis of testes in Chinese tongue sole.

2. Materials and methods

2.1. Luciferase reporter assay

The *dmrt1* (XM_008336192.3) 3'UTR was amplified by PCR using testis cDNA from the Chinese tongue sole and cloned to the psiCHECK™-2 Vector (Promega, USA) at *Not*I and *Xho*I. The primers for plasmids construction are shown in Table S1. Human embryonic kidney 293 T cells (HEK293T) were co-transfected with psiCHECK-dmrt1–3'UTR (20 ng μL^{-1}), mimics of nine candidate miRNAs or the negative control, respectively, by Lipofectamine® 2000 (11668–019, Invitrogen, USA). At 48 h after transfection, the cells were harvested, lysed, and assayed for luciferase activity by the Dual-Luciferase® Reporter Assay kit (E1910, Promega, USA) according to the manufacturer's instructions.

2.2. Primary cell culture of testicular cells and transfection of miRNA mimics and inhibitors

An adult male Chinese tongue sole at 6 months old was anesthetized and disinfected with 75% ethanol and then the testes were removed and washed with 75% ethanol, PBS, and Leibovitz's L-15 medium (GIBCO, USA) twice, respectively. The testes were minced into small pieces (~1 mm^3) with scissors and a razor blade in Leibovitz's L-15 medium and then subjected to digestion with 0.25% Trypsin-EDTA (Solarbio, China) for 30 min at 37 °C and neutralization with Leibovitz's L-15 medium (11415064) containing 20% fetal bovine serum (FBS, 10099141C, GIBCO, USA). After filtration and centrifugation (300 *g*, 10 min), the resulting cell pellet was resuspended and transferred into 25-cm^2 tissue culture flasks containing Leibovitz's L-15 medium (3 mL) with 20% FBS, bFGF (2 ng mL^{-1}), penicillin (1000 U), and streptomycin (1000 U). The primary cells were cultured at 24 °C and culture medium was changed every 3 days until the formation of cell monolayers. The cells were then digested and transferred into new flasks when the confluence reached ~90% (4.5×10^6) at a split ratio of 1:2. After five passages, two flasks of testicular cells were taken for verification of their initial levels of *dmrt1* and miRNAs followed by transfection of miRNA mimics or inhibitors.

Testicular cells were transferred into six-well plates with a density of 1×10^6 cells per well. When confluence was reached at 80% after 2 days, the miRNA mimics (50 nM, $n = 3$), inhibitors (50 nM, n = 3), and corresponding negative controls (NCs) (50 nM, n = 3) synthesized by GenePharma were transfected using Lipofectamine 2000 (Invitrogen, USA) according to the manufacturer's instruction. The medium was changed to regular growth medium after 6 h, and the cells were harvested for gene expression analysis after 24 h.

2.3. RNA extraction and quantitative real-time PCR

To detect the expression of genes or miRNAs in cells or tissues, total RNA was extracted using Trizol reagent (15,596,018, Invitrogen, USA) followed by integrity checking by agarose gel electrophoresis and quantification by spectrophotometry. The cDNAs of mRNA and miRNA were synthesized by the FastKing RT kit (KR116, Tiangen, China) and the miRcute Plus miRNA First-Strand cDNA kit (KR211, Tiangen, China), respectively. RT-qPCR was conducted in 384-well plates using a Talent qPCR PreMix kit (FP209, Tiangen, China) for mRNA and a MiRcute Plus miRNA qPCR kit (FP411, Tiangen, China) for miRNA in the LightCycler 480 II qRT-PCR system (Roche Diagnostics, Mannheim, Germany). Each PCR assay included replicate samples (duplicate of reverse transcription and PCR amplification) and negative controls (RT- and cDNA-free samples, respectively). All qPCR primers were validated *via* a serial dilution standard curve to have a PCR efficiency between 1.8 and 2, and melting curve analysis was conducted to confirm the specificity of the amplification reaction. The $2^{-\Delta\Delta CT}$ method was applied for relative quantification of expression levels. β-actin and U6 were used for the normalization of gene and miRNA expression, respectively. The primers used for the RT-qPCR are listed in Table S1.

2.4. Data sources

The data used for screening miRNAs targeting the 3'UTR of *dmrt1* (NM_001294232.1) in testes were obtained from the whole transcriptome sequencing data (PRJNA700834) [22]. Miranda (v3.3a) was used to predict the miRNA-binding sites in the target genes [23]. The data used for determining *dmrt1* expression in different testicular cell types and screening for the top 50 membrane receptors on Sertoli cells were obtained from single-cell RNA sequencing data (CNP0002135) [24]. The transcript counts from single-cell RNA sequencing was normalized as counts per million (CPM). The expression of membrane receptors on Sertoli cells were obtained by retaining the items including "receptor" while excluding "nuclear." By sorting in descending order according to their expression values, we listed the top 50 membrane receptors with high expression. Furthermore, the expression profiles of the top 50 membrane receptors in brain, testis, liver, and muscle of Chinese tongue sole at the age of 4 months and 1 year were obtained from whole transcriptome sequencing data (PRJNA724919). After trimming off the adapter, poly-N, and low-quality reads, the clean reads were mapped to the reference genome (RefSeq GCF_000523025.1) and the gene expression was quantified using Stringtie-1.3.3b. The expression of the top 50 membrane receptors was retrieved and saved for subsequent analysis. The advanced heatmap plots were produced using OmicStudio tools at https://www.omicstudio.cn. Gene expression pattern analysis was performed with Short Time-series Expression Miner software (STEM) from the OmicShare tools platform (www.omicshare.com/tools).

2.5. Establishment of the cys-FSHR-FSH complex model and analysis of interface residues

Amino acid sequences of *cys*-FSHR (NP_001281119.1), *cys*-FSHα (AFD04550.1), and *cys*-FSHβ (XP_024909479.1) were utilized for the construction of a *cys*-FSHR-FSH complex model by Alphafold-Multimer [25]. The results were evaluated by multiple sequence alignment (MSA), predicted local distance difference test (pLDDT), and predicted alignment error (PAE). All structure figures and the residues at the interface between *cys*-FSHR and *cys*-FSH were prepared and analyzed by PyMOL (the PyMOL Molecular Graphics System, Version 2.0, Schrödinger, LLC). The transmembrane domains were predicted with TMHMM server v 2.0. [26]. Amino acid sequences were aligned using the Needleman-Wunsch algorithm [27].

2.6. Primary cell culture of ovarian cells and isolation of exosomes from culture medium

Ovarian tissue was taken from a female Chinese tongue sole at 6 months of age after anesthesia. The methods used for the primary culture and subculture of ovary cells were similar to those for testicular cells. After three passages, the regular growth medium was removed and the cells were rinsed with PBS three times. Medium with 15% exosome-depleted FBS (SBI, USA) was added for exosome production and was collected for exosome isolation when the confluency reached 95% after 2 days. Differential centrifugation was used to isolate exosomes from the medium according to Théry et al. [28]. Briefly, the medium was subjected to successive centrifugations at increasing speeds to remove dead cells (300 g, 10 min) and cell debris (2000 g, 10 min) followed by filtration using 0.22-μm sterilized filters (C85052, Millipore, China). The filtrate was then ultracentrifuged for 70 min at 100,000 g, 4 °C (SW41Ti, Beckman, USA). The pellet was washed in PBS and again ultracentrifuged for 70 min at 100,000 g, 4 °C to concentrate the exosome preparation.

2.7. Characterization of exosomes-Western blotting

The samples were disintegrated by RIPA lysis buffer (R0010, Solarbio, China) and total protein was measured by the bicinchoninic acid (BCA) kit according to the manufacturer's instruction (PC0020, Solarbio, China). Protein (20 μg) was separated by sodium dodecyl sulfate polyacrylamide gel electrophoresis (SDS-PAGE) and transferred to polyvinylidene fluoride (PVDF) membranes (Millipore, China). The membranes were blocked in 5% defatted milk for 2 h at room temperature and then incubated with specific primary antibodies for 2 h at room temperature. The following primary antibodies were used in the present study: CD63 (ab134045, 1:1000 dilution, Abcam, USA), CD81 (ab109201, 1:1000 dilution, Abcam, USA), and HSP70 (ab181606, 1:1000 dilution, Abcam, USA). Then the membranes were washed three times using TBST (TBS containing 0.1% Tween-20) and incubated with a Goat Anti-Rabbit IgG H&L horseradish peroxidase–conjugated secondary antibody (ab205718, 1:4000 dilution, Abcam) for 1 h at room temperature. The proteins were visualized by chemiluminescent reagents (34,580, Thermo Fisher, Waltham, MA, US) after washing with TBST.

2.8. Characterization of exosomes: transmission electron microscopy

Exosomes were fixed on a 200 mesh carbon/formvar-coated grid by floating the grid upside down on an exosome droplet (10 μL) for 10 min. The grid was then transferred to a droplet of distilled water for 1 min and then to 2.5% glutaraldehyde for 10 min. After fixation, the absorbed exosomes were negatively stained with 2% uranyl acetate for 1 min. The grid was examined using a transmission electron microscope operated at 120 kV (HT7700, Hitachi, Japan).

2.9. Characterization of exosomes: nano-flow cytometry (nFCM) measurement

The concentration and size distribution were measured by an nFCM nanoanalyzer (NanoFCM, China) according to the manufacturer's instructions. Side scatter (SSC) and fluorescence of individual exosomes were detected by two single photon-counting avalanche photodiodes (APDs). The instrument was calibrated for concentration and size using 100-nm orange FluoSpheres of known concentrations (F8800, Invitrogen, USA). The exosome preparations were passed by the detector and then the events were recorded for 1 min. The flow rate and side-scattering intensity were converted to particle concentrations and then sizes based on the calibration curve and the fluorescence were recorded for the proportion of FITC exosomes.

2.10. Exosome membrane modification with peptides

PEP1 (FMTDHSYQGNRQQQKTCN) and PEP2 (KCNCAVCDLKT MDCGRFVET) labeled with Fluorescein Isothiocyanate (FITC) were synthesized by GenScript (Piscataway, NJ). Dioleoyl phosphatidylethanolamine-N-hydroxysuccinimide (DOPE-NHS, Ruixi Biological Technology, China) and peptides with 50-fold in the amount of substance reacted for 1 h to form DOPE-PEP1 and DOPE-PEP2, respectively. Then 5 μL of 0.1-mM DOPE-PEP1 and DOPE-PEP2 were incubated with 1-mL exosomes (1.69×10^9 particles mL^{-1}) for 1.5 h at room temperature to obtain Exo-PEP1 and Exo-PEP2. After exosome purification and concentration using Amicon centrifugal filter devices (UFC210024, Millipore, China) twice, the modified exosomes were subjected to modifying efficiency detection by an nFCM nanoanalyzer (NanoFCM, China) as described previously.

2.11. Tracking of exosomes: In vitro

Exo (unmodified exosomes), Exo-PEP1 (exosomes modified with PEP1), and Exo-PEP2 (exosomes modified with PEP2) were labeled with 1-μM 1,1′-dioctadecyl-3,3,3′,3′-tetramethylindocarbocyanine perchlorate (DiI, V22885, Invitrogen, USA) for 20 min according to the manufacturer's instructions. The dyed exosomes were washed and resuspended in PBS of the initial volume by Amicon centrifugal filter devices (UFC210024, Millipore, China) to remove the unbound DiI before concentration detection as described previously. When the testicular cells reached 70% confluence, the regular growth medium was removed and the culture medium containing exosome-depleted FBS was added after rinsing cells three times with PBS. The testicular cells were incubated with the DiI labeled Exo, Exo-PEP1, and Exo-PEP2 (3.5×10^7 particles mL^{-1}), respectively, at 24 °C for 12 h. The cells were then fixed in 4% paraformaldehyde for 20 min, rinsed with PBS for three times, and stained with DAPI (C1005, Beyotime Biotechnology, China) for 5 min. The images were captured using an inverted microscope system (OLYMPUS, IX73, Japan). Fluorescence quantification was performed by Image J [29].

2.12. Tracking of exosomes: In vivo

A total of 1-μM 1,1-dioctadecyl-3,3,3,3-tetramethylindotricarbocyanine iodide (DiR, D12731, Invitrogen, USA) was used to label Exo, Exo-PEP1, and Exo-PEP2 at room temperature for 30 min. Excess DiR and ethanol was removed by Amicon centrifugal filter devices (UFC210024, Millipore, China). To compare the biodistribution of Exo, Exo-PEP1, and Exo-PEP2 in male fish, the DiR-labeled exosomes (1.3×10^6 particles g^{-1}) were intraperitoneally injected into fish ($n = 3$, 19.9 ± 1.32 cm). At 8 h after injection, the fish were euthanized with benzocaine (0.0375 g L^{-1}, B0600000, Sigma-Aldrich, Darmstadt, Germany) and the fluorescence images of the whole body and organs (heart, liver, spleen, intestine, and testis) were recorded by IVIS (Vilber, NEWTON 7.0, France). The fluorescence quantification was analyzed by Kuant 2.0 software

(Vilber, France). A region of interest (ROI) was drawn around each organ on each image. The ROI area and mean signal intensity were calculated.

2.13. miRNA transfection into exosomes

The ipu-miR-124a_R + 1 mimics were synthesized by GenePharma. Isolated exosomes were incubated with Exo-Fect™ (EXFT10A-1, SBI, USA) and miRNA mimics at 37 °C for 10 min and then placed on ice for 30 min followed by PBS washing and reconcentration. The resultant exosomes were subjected to succeeding experiments including membrane modification, qPCR, and animal experiments. The transfection mixtures without adding transfect reagent (BExo) or miRNA mimics (Exo) were used as controls to compare with the transfected exosomes (TExo) and TExo followed by peptide modification (PTExo) to confirm the transfection efficiency using qPCR analysis.

2.14. Animal experiment (intraperitoneal injection of exosomes)

Healthy juvenile Chinese tongue sole at age 3 months (1.27 ± 0.30 g) were purchased from Laizhou Mingbo Aquatic Co., Ltd., in Yantai, China. Chinese tongue sole males were used after genetic sex identification according to the method described previously (Fig. S1) [30]. Three dosage levels were set for the intraperitoneal injection of the engineered exosomes (2-, 4-, and 6-μg of exosome protein per gram of fish body weight) and designated as 2MPE, 4MPE, and 6MPE, respectively, according to a recent review of dosing strategy in which the median dose for EV *in vivo* injection was 2.75 μg of EV protein per gram of body weight [31]. Further, we also established two other groups injected with regular exosomes (Exo) or PBS as controls. Accordingly, 100 fish were distributed randomly into five groups (2MPE, 4MPE, 6MPE, Exo, PBS) with 20 fish per tank. All fish were acclimatized to the experimental conditions at 22 °C with aeration for 1 week prior to the experiment. Water quality parameters were monitored daily during the experiment. After acclimatization, the first administration was implemented by intraperitoneal injection. The testes from six fish per group were sampled after 2 days. The second administration was implemented on the day of first sampling, and the testes from the rest of the fish were sampled 5 days after the second injection. The testes of three fish of the first and second sampling were immediately frozen in liquid nitrogen and kept at −80 °C for gene and miRNA expression analyses. The testes of three fish from the 6MPE and PBS groups of the second sampling were immediately frozen in liquid nitrogen for RNA sequencing analyses. Furthermore, the testes of three fish from the 6MPE and PBS groups of the second sampling were washed with PBS and fixed with 4% paraformaldehyde for histological analyses.

2.15. Whole transcriptome and small RNA sequencing analyses

Testes of 6MPE and PBS from the second sampling were used for RNA library construction. Total RNAs from the testes of each fish were extracted using TRIzol reagent (Invitrogen) according to the manufacturer's procedure. The library was quantified by an Agilent 2100 bioanalyzer to meet the effective concentration higher than 2 nM. Three biological replicates for each group were generated. After the libraries were qualified, the different libraries were sequenced by the Illumina NovaSeq 6000. Clean reads were obtained by trimming reads containing adapter, poly-N, or with low quality from raw data. Q20, Q30, and GC content of the clean reads were calculated (Table S6). Clean reads were then mapped to the reference genome (RefSeq GCF_000523025.1). Gene expression was quantified by counting the read numbers mapped to each gene using Stringtie-1.3.3b. Differential expression analysis of two samples was performed using the edgeR R package (3.22.5). The *P* values were adjusted using the Benjamini and Hochberg method. Significantly differential expression genes were screened based on the corrected *P*-value (< 0.05). The data have been deposited in the NCBI Sequence Read Archive (SRA) repository (PRJNA938023).

2.16. Histological analyses

To investigate alteration of the testes after engineered exosome injection, histological analyses were conducted. Hematoxylin-eosin (H&E) staining on testes sections of 6MPE and PBS from the second sampling was performed according to standard H&E staining protocols. Testes were dissected and fixed in 4% paraformaldehyde for 24 h. Samples were dehydrated by increasing concentration of ethanol solutions and embedded in paraffin. Serial sections with thickness of 4 to 6 μm were performed and stained with hematoxylin-eosin. TUNEL analysis was performed using the TUNEL Apoptosis Assay Kit (C1088, Beyotime Biotechnology, China) following the manufacturer's instructions.

2.17. Statistical analyses

Data are presented as the means ± SD. All data were statistically analyzed by SPSS 26.0 (SPSS, Chicago, IL, USA). Student's *t*-test was performed to compare the values between two experimental groups. One-way ANOVA was performed for multiple comparisons followed by Tukey's multiple-range test. *P*-values <0.05 were considered statistically significant.

3. Results

3.1. Inhibition of dmrt1 expression by ipu-miR-124a_R + 1 (isomiR-124a)

To identify the miRNAs inhibiting expression of *dmrt1* in Chinese tongue sole, we screened for miRNAs with miRanda scores higher than 140 and binding sites distributed evenly in the 3'UTR of *dmrt1* according to the data from previous miRNA sequencing analyses [22]. Specifically, the miRNAs included four novel identified miRNAs (PC-5p-163042_37, PC-5p-120619_66, PC-5p-436116_5, PC-5p-280962_12), three isomiRs (ola-miR-338-5p_R-4_2ss13GA19CT, ipu-miR-124a_R + 1, ipu-miR-737_L-1_1ss2TG), and two mature miRNAs (ssa-miR-338a-4-5p, ola-miR-223). Among them, PC-5p-436116_5 and PC-5p-280962_12 were each predicted to have two different binding sites in the 3'UTR of *dmrt1* (Table 1 and Fig. 1A).

The interaction between the putative miRNAs and *dmrt1* 3'UTR were investigated using the dual-luciferase reporter assay in HEK 293 T cells. Results showed that the relative luciferase activities were significantly inhibited by PC-5p-163042_37, ipu-miR-124a_R + 1, and PC-5p-280962_12, indicating their potential for inhibiting *dmrt1* expression by binding to *dmrt1* 3'UTR (Fig. 1B).

To verify the negative regulation of *dmrt1* by the miRNAs, we performed primary cell culture of testicular cells from Chinese tongue sole. Expressions of PC-5p-163042_37, ipu-miR-124a_R + 1, and PC-5p-280962_12 were first detected in the fifth passage of the testicular cells and compared with those in the testis and ovary of the Chinese tongue sole at age 1 year. Results showed that the three miRNAs were all expressed higher in the fifth passage of the testicular cells and the testis than in the ovary. However, the expressions of PC-5p-163042_37 and PC-5p-280962_12 in testicular cells were significantly lower than those in the testis (Fig. 1C).

Next, a loss and gain of function of miRNAs experiment was conducted by transfection of the mimics and inhibitors of PC-5p-163042_37,

Table 1
miRNAs predicted to target the 3'UTR of *dmrt1* in the testis of Chinese tongue sole.

miRNA	Sequence 5′ → 3'	Length	Score	Energy
PC-5p-163042_37	tGCACAGGGAGGATCTAACggagag	26	165	−20.72
PC-5p-120619_66	cAACAATTAAGAGATATTTCcg	23	163	−8.68
ola-miR-338-5p_R-4_2ss13GA19CT	aACAACATCCTGATGCTGtct	22	161	−18.81
PC-5p-436116_5	cAGGAAAAGGAAACAGACAGacatt	26	159	−19.7
ssa-miR-338a-4-5p	aACAACATCCTGGTGCTGcctgagt	26	157	−20.75
ipu-miR-124a_R + 1	tAAGGCACGCGGTGAATGcca	22	156	−17.7
PC-5p-280962_12	tTAGTGAAGTCATTTATGgtct	23	155	−9.28
PC-5p-280962_12	tTAGTGAAGTCATTTATGGTct	23	153	−16.07
ola-miR-223	tGTCAGTTTGTCAAATACcc	21	152	−12.27
ipu-miR-737_L-1_1ss2TG	gTTTTTTAGGTTTTGATTttt	22	151	−10.01
PC-5p-436116_5	cAGGAAAAGGAAACAGACAGACatt	22	140	−11.94

PC-5p-280962_12, ipu-miR-124a_R + 1, and negative controls, and the expression of *dmrt1* was investigated after 24 h. The results showed that the mimics of ipu-miR-124a_R + 1 and PC-5p-280962_12 significantly inhibited the expression of *dmrt1*, and the inhibitors of ipu-miR-124a_R + 1 and PC-5p-163042_37 significantly promoted the expression of *dmrt1* (Fig. 1D, E, F). Taken together, ipu-miR-124a_R + 1 was demonstrated as an efficient negative regulator of *dmrt1*. For convenience, we will refer to ipu-miR-124a_R + 1 as isomiR-124a.

3.2. Identification of FSHR as a specific receptor in the Chinese tongue sole testis

According to a recent investigation on the testis of Chinese tongue sole by single-cell RNA sequencing analysis [24], the expression profile of *dmrt1* was extracted from seven types of testicular cells including Leydig cells, Sertoli cells, undifferentiated spermatogonia (Undiff SPG), differentiated spermatogonia (Diff SPG), preleptotene spermatocytes (Pre-Lep), pachytene spermatocytes (P-SPC), and sperm in both male and sex-reversed (WZ) pseudomale fish. Results showed that *dmrt1* was more highly expressed in the Sertoli cells of both male and pseudomale fish (Fig. 2A). Therefore, we next focused on the membrane receptors of Sertoli cells to find an optimal target for engineered exosomes. The top 50 highest expressed membrane receptors on Sertoli cells were then obtained from the dataset of the single-cell RNA sequencing (Fig. 2B and Table S2). We investigated the expression profile of the top 50 receptors in four tissues (brain, testis, liver, and muscle) at two developmental stages of fish (4-month-old juvenile fish and 1-year-old adult fish) based on the RNA sequencing data (PRJNA724919) (Fig. 2B and Table S3). According to the results of gene expression pattern analysis (Table S4), the membrane receptors with specifically high expression in the testis were displayed in profiles 13 and 14, including *fshr* (follicle-stimulating hormone receptor), *adgra3* (adhesion G protein-coupled receptor A3), *tnfrsf6* (tumor necrosis factor receptor superfamily member 6), *il17ra* (interleukin 17 receptor A), *il15ra* (interleukin 15 receptor subunit alpha), *pigr* (polymeric immunoglobulin receptor-like), and *lpar2* (lysophosphatidic acid receptor 2-like) in juvenile fish, and *fshr*, *il1r2* (interleukin 1 receptor type 2), *adgra3*, and *csf3r* (colony-stimulating factor 3 receptor), *pigr*, *trfrsf6*, and *il17ra* in adult fish. Among them, *fshr*, *pigr*, *adgra3*, *tnfrsf6*, and *il17ra* were specifically expressed in the testis at both developmental stages, and *fshr* was the one with the highest expression in Sertoli cells (Fig. 2B). Furthermore, the expression profile of *fshr* in 11 tissues validated its testis-specific expression in 6-month-old male fish as well (Fig. 2C). Taken together, we found that FSHR is a testis-specific membrane receptor with high expression on Sertoli cells of Chinese tongue sole and thus could be utilized as an optimal target for engineered exosomes.

3.3. Establishment of cys-FSHR-FSH complex structure and identification of peptides targeting cys-FSHR

To identify short peptides with strong affinity to FSHR in Chinese tongue sole (*Cynoglossus semilaevis*, *cys*), it was necessary to establish the structure of *cys*-FSHR with its natural ligand *cys*-FSH. The Alphafold-Multimer was utilized to establish the structure of the *cys*-FSHR-FSH complex. As a result, five models were well structured according to the evaluation parameters of the Alphafold-Multimer. Since Model 1 was the most confident model with the highest average predicted local distance difference test (pLDDT), we next utilized Model 1 for further analysis (Fig. S2 and Supporting Information). According to the structure of Model 1 colored by the pLDDT scale, we found that the main body of the *cys*-FSHR-FSH complex was in high confidence. In contrast, the N- or C-terminus of *cys*-FSHR and *cys*-FSH presented as the curly segments extending out of the main body was in low confidence (Fig. 3A). After computationally trimming off the N- or C-terminus with low confidence (pLDDT <70) in Model 1, the *cys*-FSHR-FSH complex showed a typical structure of glycoprotein hormone receptor, composed of an extracellular domain for recognition and binding with *cys*-FSH and a transmembrane domain. The extracellular domain of *cys*-FSHR was like a right hand in a mitten holding the *cys*-FSH (Fig. 3B).

The residues at the interface between *cys*-FSHR and *cys*-FSH in Model 1 were then analyzed by Pymol (InterfaceResidues). In total, there were 31 residues in *cys*-FSHα and 17 residues in *cys*-FSHβ located at the interface in the *cys*-FSHR-FSH complex. There were 22, 17, and 16 residues in *cys*-FSHR located at the interface between *cys*-FSHR and *cys*-FSHα, *cys*-FSHR and *cys*-FSHβ, and *cys*-FSHR and both subunits, respectively (Fig. S3). The pLDDT of residues at the interface in the *cys*-FSHR-FSH complex were all higher than 70 (Fig. S3), suggesting that the structure at the interface of the FSHR-FSH complex was confident, which was favorable for the subsequent analysis of binding sites. As FSHβ was responsible for specific binding to FSHR, we next focused on the residues located at the interface between *cys*-FSHR and *cys*-FSHβ. We found that the residues at the interface concentrated in two segments in *cys*-FSHβ, which were almost in alignment with the two peptides targeting *hsa*-FSHR for drug delivery in the study of mammals (Fig. S3) [32–34]. Because of the conserved structure and binding mode of the FSHR-FSH complex between humans and Chinese tongue sole (Fig. S4 and Supporting Information), it was highly likely that the two segments containing the residues at the interface in *cys*-FSHR-FSHβ would play important roles in binding to *cys*-FSHR as well. Therefore, the two segments from F90 to N107 (FMTDHSYQGNRQQQKTCN) and from K131 to T150 (KCNCAVCDLKTMDCGRFVET) in *cys*-FSHβ were selected as potential candidate peptides for targeting *cys*-FSHR and termed as *PEP1* and *PEP2*, respectively (Fig. S3). The structure of *cys*-FSHR-FSHβ showed that PEP1 and PEP2 were the segments that were protruding from *cys*-FSHβ into the "palm" of *cys*-FSHR. Five residues in PEP1,

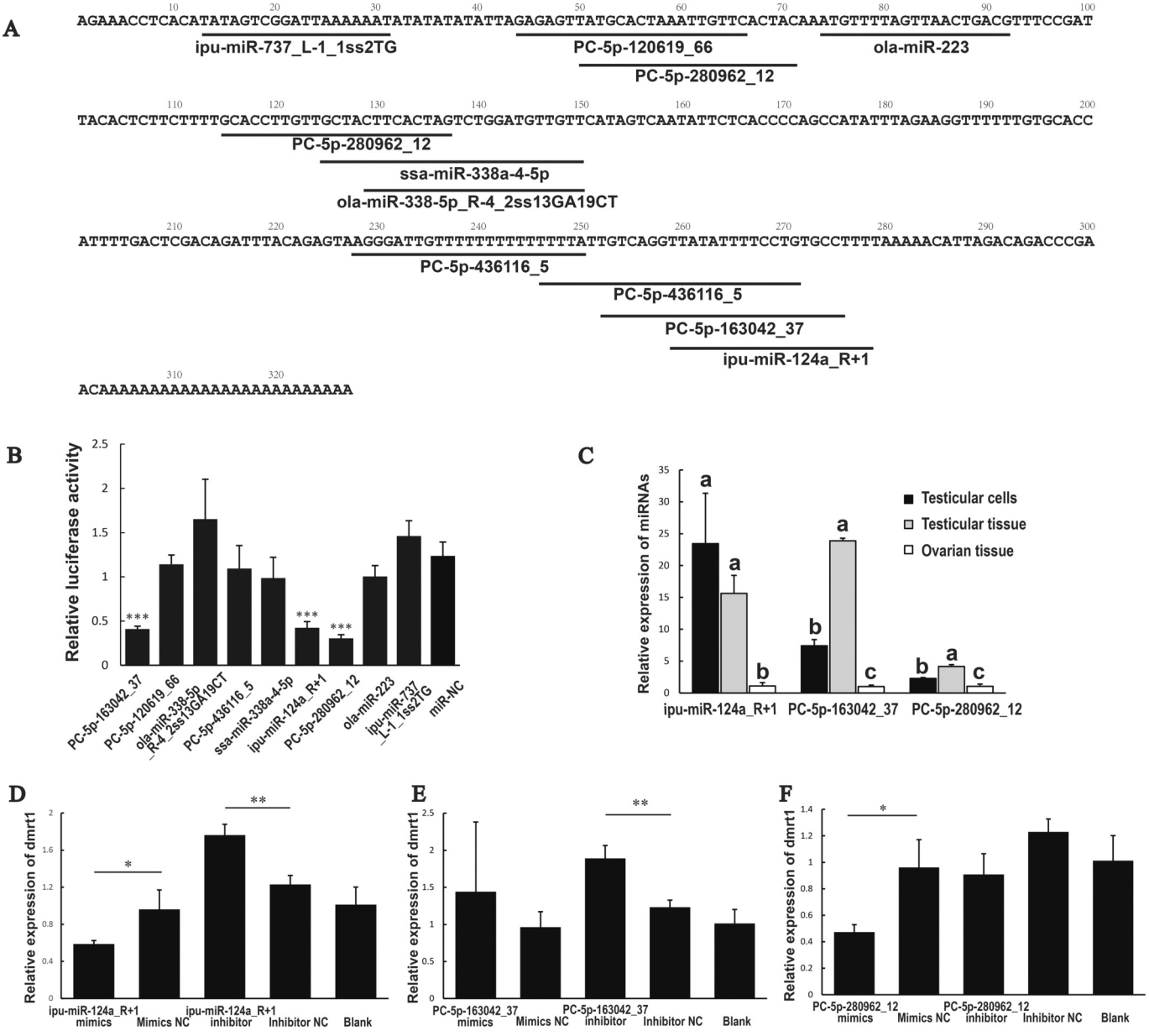

Fig. 1. Screening miRNAs inhibiting the expression of *dmrt1*. (A) Schematic representation of predicted miRNA-binding sites of nine miRNAs in the 3'UTR of *dmrt1*. (B) Relative luciferase activity in HEK293T cells transfected with psiCHECK-*dmrt1*–3'UTR, candidate miRNA mimics, and negative control mimics after 48 h. Luciferase activities were measured by dual-luciferase assays, and representative data of three independent experiments are shown as a fold ratio (renilla/firefly luciferase light-unit ratio). Values are means ($n = 3$), with standard deviations represented by vertical bars. *** Mean values with three asterisks are highly significant ($P < 0.001$, Student's *t*-test, Tukey's test). (C) Expression of ipu-miR-124a_R + 1 (isomiR-124a), PC-5p-163042_37, and PC-5p-280962_12 in testicular cells, as well as testicular and ovarian tissues. Expression values were normalized by U6. Values are means ($n = 3$), with standard deviations represented by vertical bars. [a, b, c] Mean values with unlike letters are significantly different ($P < 0.05$, one-way analysis of variance, Tukey's test). (D) Expression of *dmrt1* in the fifth passage of testicular cells of Chinese tongue transfected with ipu-miR-124a_R + 1 (isomiR-124a) mimics, mimics negative control (NC), ipu-miR-124a_R + 1 (isomiR-124a) inhibitor, and inhibitor negative control (NC) after 24 h. Expression values were normalized by U6. Values are means ($n = 3$), with standard deviations represented by vertical bars. * Mean values with one asterisk are significant (P < 0.05, Student's *t*-test, Tukey's test). ** Mean values with two asterisks are highly significant ($P < 0.01$, Student's t-test, Tukey's test). (E) Expression of *dmrt1* in the fifth passage of testicular cells of Chinese tongue transfected with PC-5p-163042_37 mimics, mimics negative control (NC), PC-5p-163042_37 inhibitor, and inhibitor negative control (NC) after 24 h. Expression values were normalized by U6. Values are means ($n = 3$), with standard deviations represented by vertical bars. ** Mean values with two asterisks are highly significant (P < 0.01, Student's *t*-test, Tukey's test). (F) Expression of *dmrt1* in the fifth passage of testicular cells of Chinese tongue transfected with PC-5p-280962_12 mimics, mimics negative control (NC), PC-5p-280962_12 inhibitor, and inhibitor negative control (NC) after 24 h. Expression values were normalized by U6. Values are means (n = 3), with standard deviations represented by vertical bars. * Mean values with one asterisk are significant ($P < 0.05$, Student's t-test, Tukey's test).

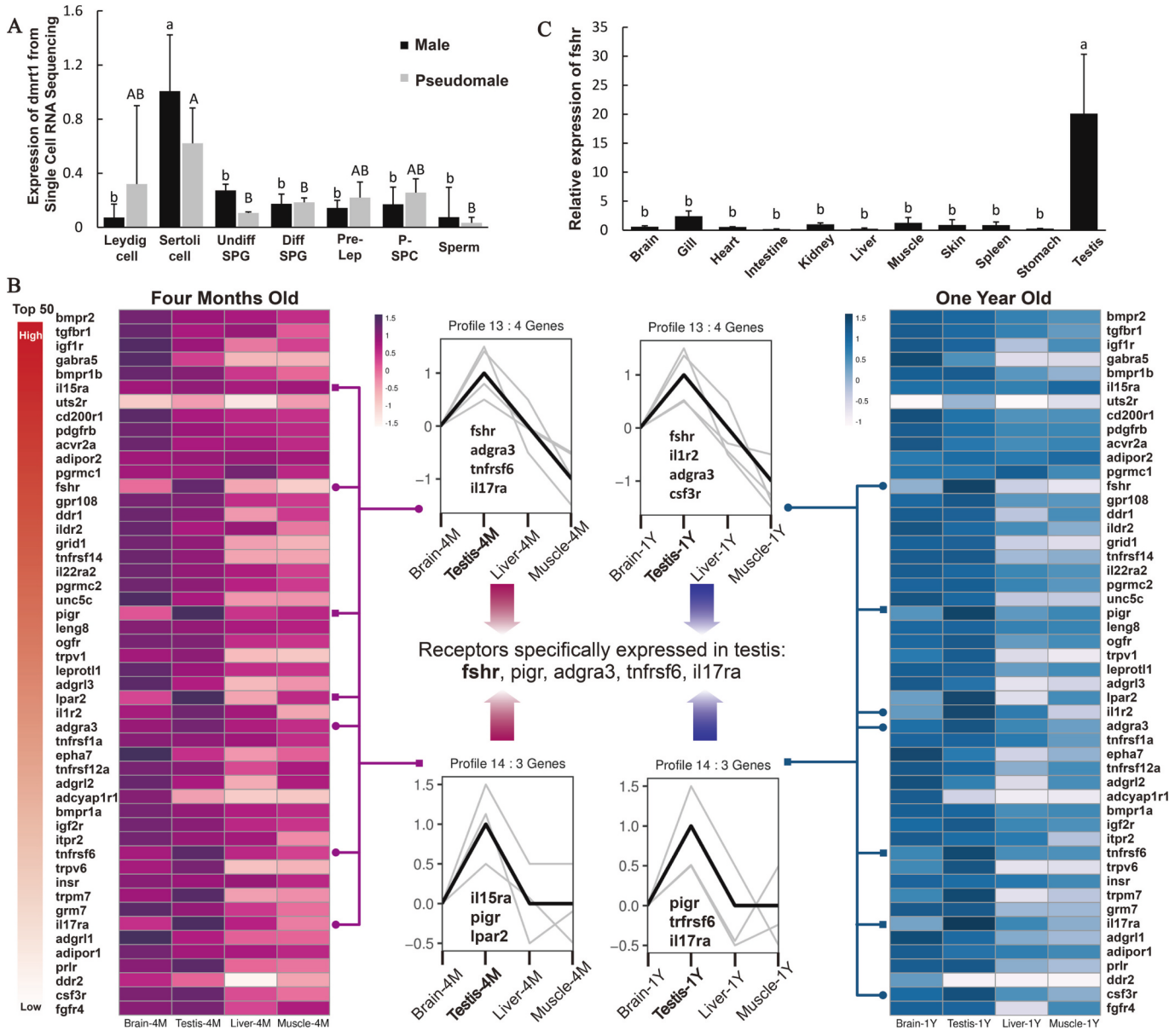

Fig. 2. Screening for membrane receptors specifically expressed in testes of Chinese tongue sole. (A) Expression of *dmrt1* in seven types of testicular cells, including Leydig cells, Sertoli cells, undifferentiated spermatogonia (Undiff SPG), differentiated spermatogonia (Diff SPG), preleptotene spermatocytes (Pre-Lep), pachytene spermatocytes (P-SPC), and sperm. The data was extracted from the single-cell RNA sequencing analysis data (CNP0002135) of both male and pseudomale of 2-year-old Chinese tongue sole. Values are means ($n = 3$), with standard deviations represented by vertical bars. [a, b] Mean values with unlike lowercase letters are significantly different in male fish. [A, B] Mean values with unlike uppercase letters are significantly different in pseudomale fish ($P < 0.05$, one-way analysis of variance, Tukey's test). (B) Top 50 highest expressed membrane receptors on Sertoli cells extracted from the dataset of single-cell RNA sequencing (CNP0002135) and their expression profile in brain, testis, liver, and muscle of Chinese tongue sole at 4 months old (in magenta heatmap) and 1 year old (in blue heatmap) extracted from RNA sequencing data (PRJNA724919). After gene expression pattern analysis, the membrane receptors from profiles 13 (marked by dots) and 14 (marked by squares) characterized by specifically higher expression in the testis were displayed. Fshr (follicle stimulating hormone receptor), adgra3 (adhesion G protein-coupled receptor A3), tnfrsf6 (tumor necrosis factor receptor superfamily member 6), il17ra (interleukin 17 receptor A), il15ra (interleukin 15 receptor subunit alpha), pigr (polymeric immunoglobulin receptor-like), lpar2 (lysophosphatidic acid receptor 2-like), il1r2 (interleukin 1 receptor type 2), and csf3r (colony-stimulating factor 3 receptor). (C) Expression of *fshr* in brain, gill, heart, intestine, kidney, liver, muscle, skin, spleen, stomach, and testis of 6-month-old Chinese tongue sole. Expression values were normalized by *β-actin*. Values are means ($n = 3$), with standard deviations represented by vertical bars. [a, b] Mean values with unlike letters are significantly different ($P < 0.05$, one-way analysis of variance, Tukey's test). (For interpretation of the references to colour in this figure legend, the reader is referred to the web version of this article.)

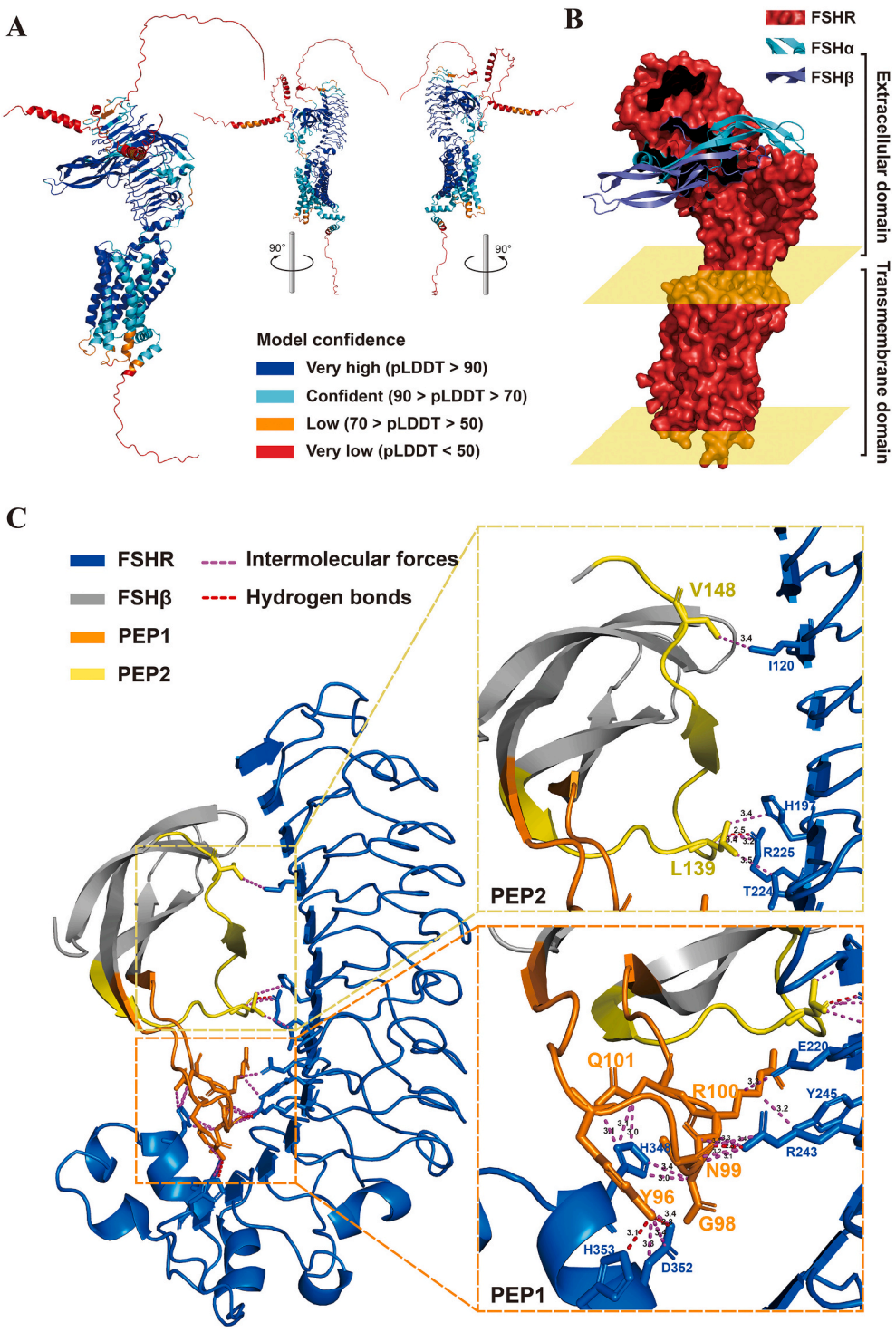

Fig. 3. Structure of the *cys*-FSHR-FSH complex and peptides at the interface. (A) Complete structure of the *cys*-FSHR-FSH complex in Model 1. Each residue is colored based on pLDDT. (B) Structure of the *cys*-FSHR-FSH complex in Model 1 after trimming off residues at the N- and C-terminus with low confidence (pLDDT <70) in Model 1. Extracellular and transmembrane domains were segmented with yellow plates schematically. *Cys*-FSHα and *cys*-FSHβ are shown in a cartoon fashion in cyan and blue, and *cys*-FSHR is shown in a surface fashion in red. (C) Extracellular structure and binding sites of *cys*-FSHR-FSHβ. The structures of *cys*-FSHR and *cys*-FSHβ are shown in a cartoon fashion in blue and gray, respectively. The PEP1 and PEP2 in *cys*-FSHβ-containing binding sites are shown in a stick fashion in orange and yellow, respectively. Intermolecular forces and hydrogen bonds with bond lengths are shown between residues of *cys*-FSHβ and *cys*-FSHR.

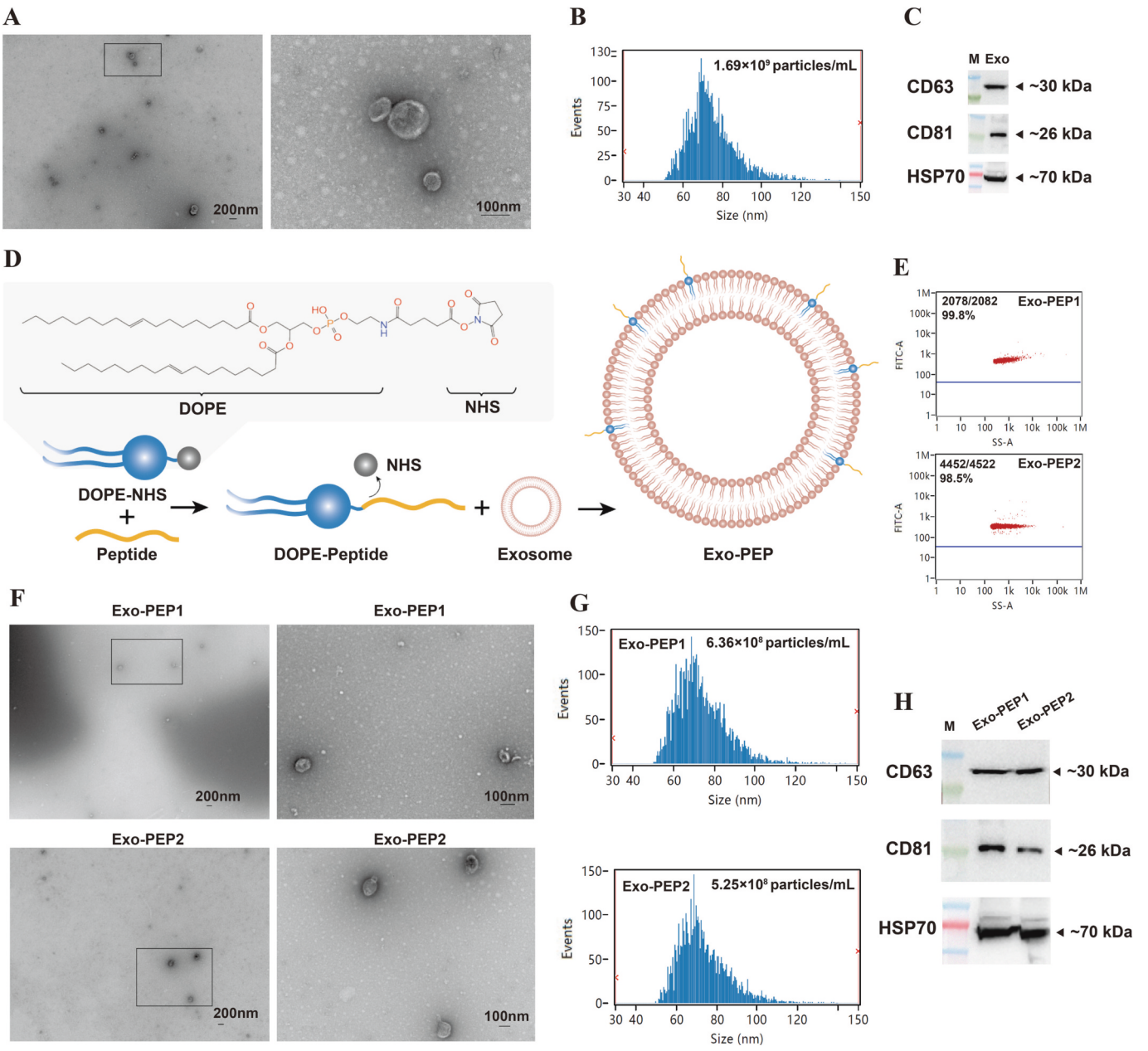

Fig. 4. Characterization of exosomes derived from ovarian cells and modification of peptides. (A) Morphology of exosomes isolated from ovarian cells viewed by transmission electron microscopy with wide-field (left) and close-up (right) images. (B) Particle size distribution and concentration of exosomes isolated from ovarian cells analyzed by Nano-FCM. (C) Western blotting examination of exosomal biomarkers (CD63, CD81, and HSP70) in exosomes isolated from ovarian cells. (M: marker; Exo: exosomes isolated from the ovarian cells). (D) Schematic diagram illustrating the exosome modification with peptides. DOPE-NHS is a double-lipid anchor modified with NHS that is amino reactive. DOPE-NHS and peptides reacted to form DOPE-peptides that are able to insert into the exosomal membrane spontaneously. (DOPE: dioleoylphosphatidylethanolamine; NHS: N-hydroxysuccinimide; Exo-PEP: exosomes modified with peptides). (E) Efficiency of exosomal modification with PEP1 (up) and PEP2 (down). PEP1 and PEP2 labeled with Fluorescein Isothiocyanate (FITC) were used for exosomal modification, and the modified exosomes (Exo-PEP1 and Exo-PEP2) with FITC labeling were detected and analyzed by Nano-FCM. (F) Morphology of exosomes modified with PEP1 (top) and PEP2 (bottom) viewed by transmission electron microscopy with wide-field (left) and close-up (right) images. (G) Particle size distribution and concentration of exosomes modified with PEP1 (top) and PEP2 (bottom) analyzed by Nano-FCM. (H) Western blotting examination of exosomal biomarkers (CD63, CD81, and HSP70) from exosomes modified with PEP1 and PEP2. (M: marker; Exo-PEP1: exosomes modified with PEP1; Exo-PEP2: exosomes modified with PEP2).

including Y96, G98, N99, R100, and Q101, and two residues in PEP2, including L139 and V148, were the most likely residues binding to *cys*-FSHR directly based on analysis of intermolecular forces and hydrogen bonds (Fig. 3C).

3.4. Exosome preparations and membrane modification with peptides

Ovarian cells were cultured for exosome preparation to increase tropism to gonad and avoid incorporating male-triggering substances. Exosomes were isolated from the medium of the third passage of ovarian cells. The morphology of exosomes observed by TEM showed that most particles were cup shaped and in diameters of 50–200 nm (Fig. 4A). Next, the size and concentration of the exosomes were analyzed by Nano-FCM. The diameter of the exosomes displayed a normal distribution ranging from 50.75 to 134.25 nm with an average diameter of 74.81 nm, and the concentration was 1.69×10^9 particles mL^{-1} (Fig. 4B). Exosomal marker proteins [35] including CD63 (~30 kDa), CD81 (~26 kDa), and HSP70 (~70 kDa) were also identified in the

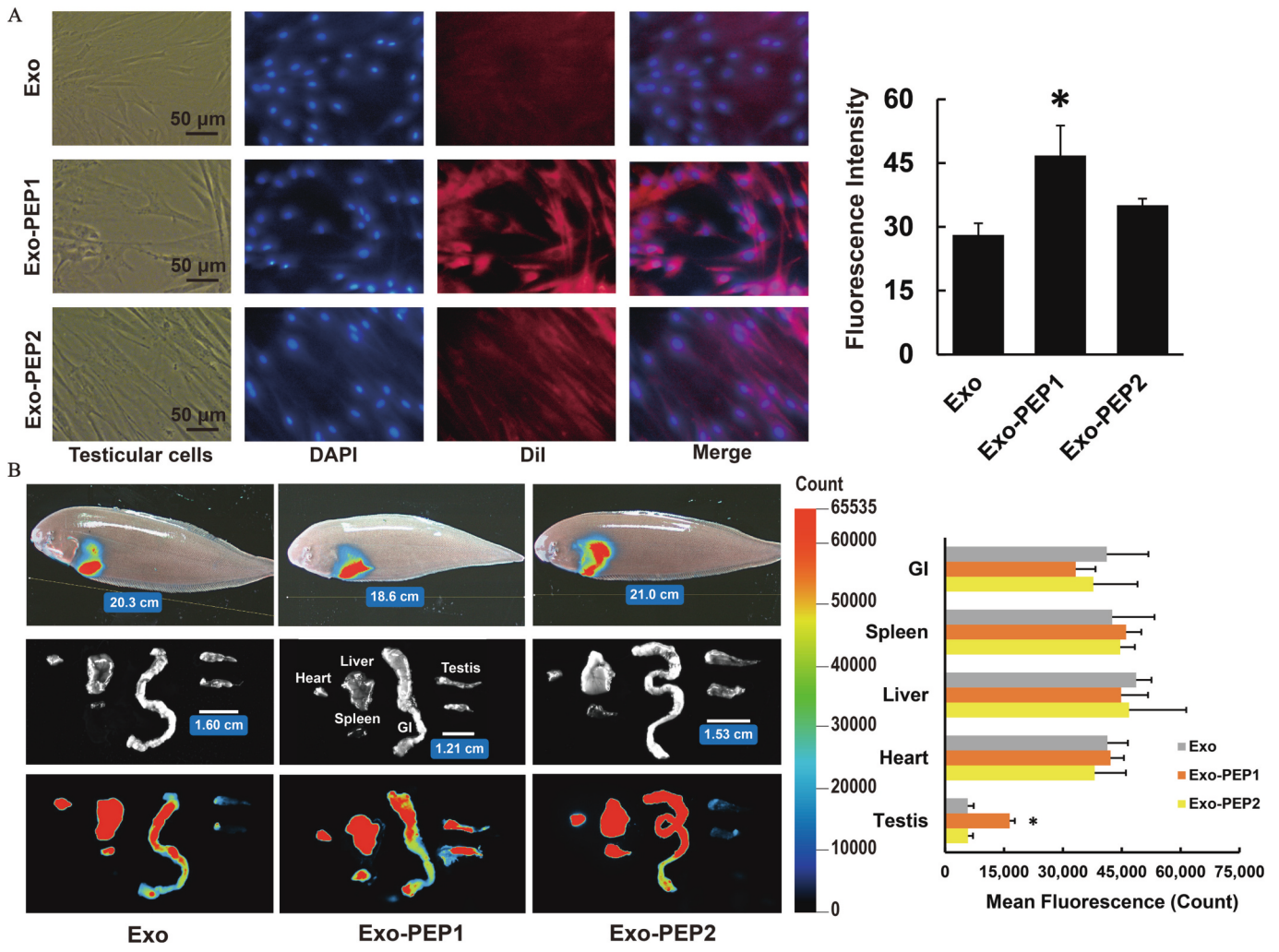

Fig. 5. Testis-targeting efficiency of exosomes modified with PEP1 and PEP2 *in vitro* and *in vivo*. (A) Representative images of testicular cells incubated with DiI-labeled exosomes (Exo) and DiI-labeled exosomes modified with PEP1 (Exo-PEP1) and PEP2 (Exo-PEP2) after 12 h (left). Fluorescence intensity was quantified by Image J (right). Values are means ($n = 3$), with standard deviations represented by vertical bars. * Mean values with one asterisk are significantly different ($P < 0.05$, one-way analysis of variance, Tukey's test). (B) Representative images of distribution of DiR-labeled exosomes (Exo) and DiR-labeled exosomes modified with PEP1 (Exo-PEP1) and PEP2 (Exo-PEP2) in Chinese tongue sole whole fish (left top) and organs (left bottom) 8 h after intraperitoneal injection. The fluorescence count was recorded and analyzed by Kuant 2.0 (right). Values are means (n = 3), with standard deviations represented by vertical bars. * Mean values with one asterisk are significantly different ($P < 0.05$, one-way analysis of variance, Tukey's test) (GI: gastrointestinal tract).

exosomes isolated from the ovarian cells (Fig. 4C).

We then modified the exosomes with PEP1 and PEP2 labeled with FITC through DOPE-NHS linkers (Fig. 4D). The efficiency of exosomal modification with peptides was assessed by Nano-FCM. Results showed that the proportion of modified exosomes was 99.8% and 98.5% for Exo-PEP1 and Exo-PEP2, respectively, indicating that the majority of exosomes were modified with PEP1 and PEP2 successfully (Fig. 4E). Furthermore, the morphology of Exo-PEP1 and Exo-PEP2 was investigated. Results showed that they were still in a cuplike shape with average diameters of 74.11 and 73.25 nm, respectively, which are not much different from the original sizes of exosomes. However, the final concentration of Exo-PEP1 and Exo-PEP2 were 6.10×10^8 and 5.25×10^8 particles mL^{-1}, respectively, indicating that the process of exosomal modification and purification inevitably resulted in some loss of exosomes (Fig. 4F, G). Still, the exosomal marker proteins (CD63, CD81, and HSP70) were identified in Exo-PEP1 and Exo-PEP2 (Fig. 4H).

3.5. Testis-targeting effect of exosomes modified with PEP1 and PEP2 in vitro and in vivo

Next, we compared the testis-targeting efficiency of exosomes modified with PEP1 (Exo-PEP1) and PEP2 (Exo-PEP2) with the original exosomes (Exo) *in vitro* and *in vivo*. Exo, Exo-PEP1, and Exo-PEP2 labeled with DiI were used for the *in vitro* experiment. After incubation with the exosomes for 12 h, testicular cells incubated with Exo-PEP1 showed significantly higher fluorescence intensity than those incubated with Exo and Exo-PEP2, indicating that the exosomes modified with PEP1 were more preferentially absorbed by testicular cells of Chinese tongue sole (Fig. 5A). To investigate the targeting efficiency for testis tissues *in vivo*, DiR was used to label Exo, Exo-PEP1, and Exo-PEP2. The fluorescence images of the whole fish and the testes from Chinese tongue sole were recorded 8 h after intraperitoneal injection. The heart, liver, spleen and gastrointestinal tract all showed strong fluorescence regardless of the peptide modification. Similar to the *in vitro* experiment, fluorescence of the testes of fish injected with Exo-PEP1 was stronger than that of fish injected with Exo and Exo-PEP2 (Fig. 5B), suggesting that the exosomes modified with PEP1 were more efficient in targeting the testis of Chinese tongue sole.

3.6. Effect of engineered exosomes on the testis in juvenile fish

After preparations of PEP1 modified engineered exosomes

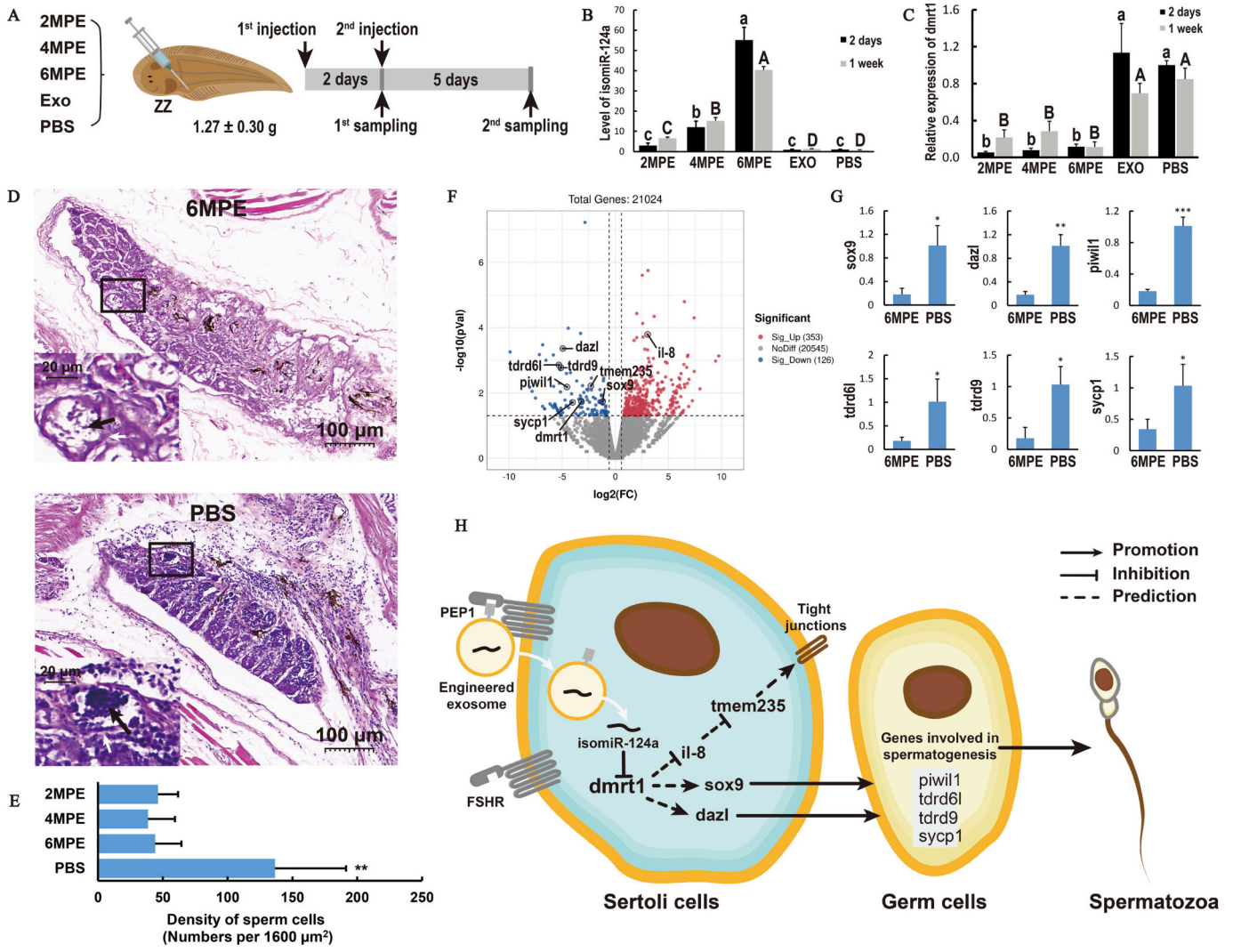

Fig. 6. Effect of engineered exosomes on testis structure and function in juvenile male fish. (A) Schematic diagram illustrating two intraperitoneal injections of engineered exosomes in juvenile male fish and sampling after injection. Juvenile fish at 3 months old (1.27 ± 0.30 g) were injected with three levels of engineered exosomes (2, 4, and 6 μg exosome protein per gram of fish body weight), designated as 2MPE, 4MPE, and 6MPE, respectively. For the control, fish were also injected with regular exosomes (Exo) and PBS. (B) Levels of isomiR-124a in the testes of fish injected with 2MPE, 4MPE, 6MPE, Exo, and PBS. Expression values were normalized by U6. Values are means ($n = 3$), with standard deviations represented by vertical bars. [a, b, c] Mean values with unlike lowercase letters are significantly different in testes sampled after 2 days. [A, B, C, D] Mean values with unlike uppercase letters were significantly different in testes sampled after 1 week ($P < 0.05$, one-way analysis of variance, Tukey's test). (C) Relative expression of *dmrt1* in the testes of fish injected with 2MPE, 4MPE, 6MPE, Exo, and PBS. Expression values were normalized by *β-actin*. Values are means ($n = 3$), with standard deviations represented by vertical bars. [a, b] Mean values with unlike lowercase letters were significantly different in testes sampled after 2 days. [A, B] Mean values with unlike uppercase letters were significantly different in testes sampled after 1 week ($P < 0.05$, one-way analysis of variance, Tukey's test). (D) Representative sections of testes from fish injected with 6MPE (up) and PBS (down) 1 week after intraperitoneal injection. Large magnification of the frame area is shown at the left bottom of the image (black arrow, germ cells; white arrow, Sertoli cells). (E) Density of sperm cells in the testes of fish injected with 2MPE, 4MPE, 6MPE, and PBS. Values are means ($n = 4$) with standard deviations. ** Mean values with two asterisks are highly significantly different ($P < 0.01$, one-way analysis of variance, Tukey's test). (F) Volcano plot showing the gene expression with significant differences between testes of fish injected with 6MPE and PBS after 1 week ($P < 0.05$, FC > 2) (red points: higher expression in the testes of fish injected with 6MPE; blue points: lower expression in the testes of fish injected with 6MPE; gray points: no significant differences between the two groups). (G) Relative expression of *sox9*, *dazl*, *piwil1*, *tdrd6l*, *tdrd9*, and *sycp1* in the testes of fish injected with 6MPE and PBS. Expression values were normalized by *β-actin*. Values are means (n = 3), with standard deviations represented by vertical bars. * Mean values with one asterisk are significantly different ($P < 0.05$, Student's *t*-test, Tukey's test). ** Mean values with two asterisks are highly significantly different ($P < 0.01$, Student's t-test, Tukey's test). *** Mean values with three asterisks are extremely significant ($P < 0.001$, Student's t-test, Tukey's test). (H) Schematic drawing illustrating inhibition of the male sex-determining gene *dmrt1* and spermatogenesis by engineered exosomes in testicular cells. The testicular cells are classified into somatic cells and male germ cells: the former includes Sertoli cells, Leydig cells, and so on, and the latter includes spermatocyte, spermatozoa, and so on. Sertoli cells are in close contact with the germ cells. The highest expression of *dmrt1* was found in Sertoli cells. FSHR was found to be a testis-specific membrane receptor highly expressed on Sertoli cells in Chinese tongue sole. As soon as the engineered exosomes modified with PEP1 were taken up by Sertoli cells by PEP1-FSHR interaction, isomiR-124a was released into the cytosol and inhibited the expression of its target gene *dmrt1* in Sertoli cells. The downstream genes of *dmrt1* were accordingly affected, including *sox9* and *dazl*, which are involved in the regulation of spermatogenesis, and *il-8* and *tmem235*, which are involved in the regulation of tight junctions in Sertoli cells. The changed gene expression in Sertoli cells further inhibited the expression of genes involved in spermatogenesis including *piwil1*, *tdrd6l*, *tdrd9*, and *sycp1* in germ cells, resulting in the defect of spermatogenesis and a decreased amount of spermatozoa. (For interpretation of the references to colour in this figure legend, the reader is referred to the web version of this article.)

containing isomiR-124a, the *in vivo* experiment was conducted by intraperitoneal injection. The testes were sampled 2 days after the first injection to monitor immediate effects. A second injection was done on the same day, and the testes were sampled after 5 days to investigate the long-term impact on testes (Fig. 6A). After the 1-week experiment, the level of isomiR-124a in the testes was determined. There was a similar level in the testes of fish sampled at 2 days after the first injection and 5 days after the second injection. The amounts of isomiR-124a in testes increased with the increasing dosage of engineered exosomes, suggesting that isomiR-124a was efficiently transported to the testes (Fig. 6B). Notably, expression of *dmrt1* in the testes was significantly inhibited in the fish injected with engineered exosomes. However, no significant differences were found in the expression of *dmrt1* among fish injected with different dosages of engineered exosomes (Fig. 6C).

Compared to the testes of fish injected with PBS, the testes of fish injected with engineered exosomes were more loosely organized and showed decreased amounts of spermatozoa in and at the periphery of the testes, suggesting an inactive state of testes and spermatogenesis, which was consistent with the low density of sperm cells in the testes of fish injected with engineered exosomes (Fig. 6D, E and Fig. S5).

We then analyzed the testes from 6MPE and PBS groups sampled after 1 week by RNA sequencing to obtain a comprehensive understanding of the effect of *dmrt1* expression modulation on testicular gene expression. Three libraries (ZM1, ZM2, ZM3) for 6MPE and three libraries (ZP1, ZP2, ZP3) for PBS were constructed. Among the 21,024 identified genes, there were 353 genes significantly upregulated and 126 genes downregulated in the testes of fish injected with 6MPE compared with those injected with PBS (P value <0.05, fold change >2) (Fig. 6F and Table S5). Reflecting the action of the applied isomiR-124a, expression of *dmrt1* was downregulated. The expression of many other genes involved in sex determination, testis development, and spermatogenesis also showed significant differences, such as *sox9* (SRY (sex-determining region Y)-box 9), *dazl* (deleted in azoospermia-like), *piwil1* (piwi-like RNA-mediated gene silencing 1), *tdrd6l* (tudor domain containing protein 6-like), *tdrd9* (tudor domain containing 9), *sycp1* (synaptonemal complex protein 1), *il-8* (interleukin 8-like), and *tmem235* (transmembrane protein 235-like) (Fig. 6F). In addition to *dmrt1*, gene expression analyzed by qPCR further validated that *sox9*, *dazl*, *piwil1*, *tdrd6l*, *tdrd9*, and *sycp1* were significantly inhibited in the testes injected with 6MPE (Fig. 6G). Taken together, it could be concluded that engineered exosomes targeting FSHR efficiently transported isomiR-124a to the Sertoli cells, resulting in the inhibition of the male sex-determining gene *dmrt1* and other genes involved in testis development and spermatogenesis in Chinese tongue sole, resulting in a defect of testicular structure and function (Fig. 6H).

4. Discussion

Although various master SD genes were identified in animals, the *dmrt1* gene is unique because of its repeated usage across metazoan species, such as Drosophila, nematode, amphibian, chicken, and fish, which suggests the highly conserved function of *dmrt1* in sexual development [10]. In mammals, sex change does not occur under natural conditions as long as the sex was determined during embryonic development. However, this is not the case in many fishes that showed various SD systems and thus provided good models to study SD and sexual plasticity.

We demonstrated that ipu-miR-124a_R + 1 efficiently inhibited the expression of *dmrt1*, termed as isomiR-124a for convenience. To our knowledge, this is the first miRNA that has been experimentally found to downregulate *dmrt1* expression in fish. In mice, it was reported that *dmrt1* was directly targeted by miRNA-224 in spermatogonial stem cells (SSCs) and that overexpression of miRNA-224 resulted in the downregulation of *dmrt1* and differentiation of SSCs [36]. Only a few investigations showed that some miRNAs were predicted to target *dmrt1* in fish by *in silico* methods [37–39]. As *dmrt1* plays pivotal role in evolutionary transitions of SD mechanisms in vertebrate [11], the finding of isomiR-124a as an inherent *dmrt1* suppressor has both theoretical and practical implications and warrants in-depth investigations in the future.

Consistent with the other fish examined [11], the expression of *dmrt1* was limited to the testis of Chinese tongue sole [19]. Furthermore, single-cell RNA sequencing analysis in the testes of 2-year-old Chinese tongue sole showed that *dmrt1* was significantly higher expressed in the Sertoli cells than all other cells in both male and pseudo male fish [24]. Therefore, targeting the membrane receptors on Sertoli cells could contribute to the specific delivery of isomiR-124a to the testes for efficient regulation of *dmrt1*. In the present study, we found that *fshr* was specifically expressed in the testes of fish and showed high expression in Sertoli cells, consistent with the finding in mammals [40]. Moreover, it was reported that FSHR was repeatedly used as an ovary-specific target by peptide-modified nanoparticles for precise therapy in mammalian studies [32–34], providing the references of targeting FSHR with FSHR-specific peptides. It is known that FSHR belongs to the G protein-coupled receptor (GPCR) superfamily. FSH, the natural ligand of FSHR, is a heterodimeric glycoprotein composed of an α and a β subunit, and both subunits are responsible for the interaction with FSHR. Furthermore, FSH has an α subunit identical to the other glycoproteins including luteinizing hormone (LH), chorionic gonadotropin (CG), and thyroid-stimulating hormone (TSH), but a unique β subunit is responsible for the specific binding with FSHR [40]. Therefore, pinpointing the peptides on FSHβ interacting with FSHR in the FSHR-FSH complex was the key to our work. Different from the completed structure of the FSHR-FSH complex resolved by experimental methods in human studies [41,42], the structure of the FSHR-FSH complex for Chinese tongue sole was established by Alphafold-Multimer in the present study, which is emerging as a revolutionary method for predicting the protein structure with accuracy matched with experimental determination methods [25,43]. Two peptides locating at the interface of the complex were accurately identified owing to the highly qualified establishment of the FSHR-FSH complex model.

Regarding the cells for exosomal production in the field of drug delivery, it was suggested that the extracellular vesicles could home in on their parental cells of origin *via* the same surface extracellular proteins [44]. Many studies accordingly utilized the self-derived cells as parental cells for exosome production. For example, prostate cancer cell derived exosomes loaded with Paclitaxel showed enhanced cytotoxicity after endocytosis by prostate cancer cells [45]. The neural progenitor cell derived exosomes could promote the generation and differentiation of neurons by transferring key miRNAs to neurons [46]. Given that the testis and ovary are homologous organs and the exosomal content was similar to their parental cells [1], we utilized the ovarian cell derived exosomes to increase their tropism to gonad and avoid incorporating male-triggering substances that may interfere with the *dmrt1*-suppressing effect instead of using testicular cell derived exosomes. The exosomes were then isolated from ovarian cells, showing typical characteristics of exosomes in morphology, diameters, and marker proteins, and the yield was sufficient for succeeding manipulations.

The technology for exosomal surface modification can be generally categorized into endogenous or exogenous modification according to the subject to manipulate. The exogenous modification indicates the direct modification on the exosomal surface after purification, having the merit of more tolerance and feasibility than living cells under various conditions [47]. It was reported that phospholipid membrane anchor technology was able to modify the exosomal membrane with targeting peptide by lipid anchors, known as a simple and rapid method without genetic manipulation to the exosome parental cells, being advantageous to maintain the integrity of the exosomal membrane [48–50]. Therefore, we adopted the membrane anchor technology for exosomal modification with PEP1 and PEP2 in the present study. According to the proportion of exosomes modified with either PEP1 or PEP2, most exosomes were successfully modified using membrane anchor technology. Moreover,

the exosomal morphology, diameters, and marker proteins were not changed after membrane modification with peptides, suggesting that the integrity of exosomes was not affected by peptide modification.

In the present study, the strong fluorescence in the gastrointestinal tract, spleen, liver, and heart 8 h after intraperitoneal injection was consistent with the findings in mammals [44], showing that the exosomes preferentially accumulated in these tissues after intraperitoneal injection regardless of peptide modification. This may be due to the direct contact of those organs with exosomes in the peritoneal cavity and through blood circulation. However, the fluorescence in testes was closely associated with peptide modification, showing stronger fluorescence in exosomes modified with PEP1, suggesting that the PEP1 modification was able to promote the accessibility of exosomes to testes in Chinese tongue sole. Therefore, given that the testes in flatfish extend from the peritoneal cavity to the distal end and testes were protected from the exogenous biomolecules by the blood-testis barrier (BTB) that is formed by Sertoli cells near the base of the epithelium of seminiferous tubules [51], it is necessary to modify the exosomes with PEP1 for efficient targeting to testes.

Different strategies have been developed to load small RNAs into exosomes, such as parental cell transfection [52], exosomal membrane modulation by electroporation [53], and the commercial kit Exo-Fect [54]. Among the five methods for direct modulation of EVs, Ricardo et al. found that loading miRNAs with Exo-Fect showed the most efficiency and was able to enhance the uptake of EVs by target cells and decrease the interaction of EVs with lysosomes [55]; therefore, the Exo-Fect method was used in the present study. To minimize the negative impact on peptide-modifying efficiency caused by membrane perturbation during miRNA transfection, we prepared the engineered exosomes in a fashion that miRNA mimics were loaded prior to membrane modification with peptides, which was consistent with the method reported by Gunassekaran et al. [48]. Although there was some loss of miRNA after peptide modification, the level of isomiR-124a in transfected exosomes was still significantly higher than the native exosomes. Accordingly, the engineered exosomes with miRNA transfection and then peptide modification (MPE) were well prepared for the *in vivo* experiment.

The *in vivo* experiment showed that the levels of isomiR-124a in testes were promoted with increasing dosages of engineered exosomes after injection at both sampling time points. However, the expression of *dmrt1* was significantly inhibited by the engineered exosomes independent of the dosages, suggesting that isomiR-124a could efficiently repress the expression of *dmrt1* in the testes even at a relatively low dosage. RNA sequencing analysis was performed to obtain a transcriptome-wide view of the effect of engineered exosomes on testes. In addition to *dmrt1*, the differential gene expression analysis further revealed that the key testis-determining factor in mammals, *sox9* [56], was significantly inhibited in the testes of fish injected with engineered exosomes. *Sox9* is an important member of *sox*-family genes, which are another source of master SD regulators together with the *dmrt* family [57]. It was reported that *sox9* is a direct target of the master SD gene *Sry* in mammals and is involved in the differentiation of Sertoli cells [58,59]. Moreover, studies in mammals and fish both suggested that the expression of *sox9* is regulated by *dmrt1* [21,60]. Therefore, the downregulation of *sox9* in the present study may be a direct downstream effect after the inhibition of *dmrt1*. Further experiments should be conducted to validate the relationship between *dmrt1* and *sox9* in fish.

In addition to being a master SD gene, *dmrt1* plays important roles in maintaining testis development and functions after the testes are formed. With regard to maintaining the differentiated state of the testis, *dmrt1* has been shown to be required for the proper organization of Sertoli cells. It is involved in regulating the polarization and tight junctions of this cell type [61,62]. The upregulation of interleukin 8 (IL-8), which was reported to inhibit tight junction formation [63] together with the downregulation of transmembrane protein 235 (*tmem235*) containing the conserved domain of claudin (the important protein of tight junction in testes [64]), suggested that the tight junctions in testes were affected by *dmrt1* inhibition, which may be the reason the morphology of testes in fish injected with engineered exosomes was more loosely organized.

Regarding spermatogenesis, *dmrt1* has been reported to be involved in germ cell mitosis [17] and maintenance of spermatogonial stem cells pool in mammals [65]. Moreover, *dmrt1* expression was concomitant with the appearance of spermatocytes during natural sex reversal of the protogynous wrasse [66], which suggested the important roles of *dmrt1* in spermatogenesis in fish. The decreased expression of the master translational regulator of spermatogenesis *dazl* [67] and other genes involved in spermatogenesis, including *piwil1*, *tdrd6l*, *tdrd9*, and *sycp1*, suggested the spermatogenesis was inhibited as a consequence of downmodulation of *dmrt1*. PIWI proteins belong to the germline-specific members of the Argonaute (AGO) family, which function to silence transposable elements in the germ line and sustain gonadal development by binding to PIWI-interacting RNAs (piRNAs) in animals [68]. Additionally, the PIWI proteins provide binding platforms for Tudor domain containing proteins that are involved in germ cell development mediated by the piRNA pathway [68]. In mammals, PIWIL1 has been reported to play important roles in spermatogenesis by interacting with TDRD6 and TDRD9 [69]. The higher expression of *tdrd6l* and *tdrd9* in the testes of Japanese flounder again suggested their conserved functions in spermatogenesis in teleost fish [70]. Therefore, the downregulation of *piwil1*, *tdrd6l*, and *tdrd9* suggested that the spermatogenesis mediated by the piRNA pathway was inhibited in the testes of fish injected with engineered exosomes. SYCP1 is a component of the synaptonemal complex essential for synapsis of homologous chromosomes during meiosis [71]. The decreased expression of *sycp1* also suggested that the early steps of gametogenesis were inhibited. As *dmrt1* was also reported to be involved in the continuous production of sperm by coordinating mitotic amplification with meiosis [17], this suggested another link as to how *dmrt1* suppression could directly result in the defect of spermatogenesis. Furthermore, histological analysis found that engineered exosomes resulted in fewer spermatozoa and a more loosely organized structure of testes, showing inhibited spermatogenesis and an inactive state of testes in fish injected with engineered exosomes. However, the inhibition of *dmrt1* by engineered exosomes in testes did not change the gonadal fate in Chinese tongue sole, which is similar to the results in mammals [72]. This result suggested that *dmrt1* suppression was not able to induce sexual reversal when the gonadal sex was established in gonochoric fish.

5. Conclusion

The present study took advantage of an exosome-based delivery system for efficient interfering with a master SD gene, revealing the important roles of dmrt1 in maintaining the normal structure and functions of testis in fish. This finding fills the knowledge gap of understanding the postnatal and post-SD role of dmrt1 in fish. We believe that this powerful tool is not only instrumental to investigate the molecular mechanisms of SD genes but also will play more supportive roles in addressing biological problems in more extensive fields in the future.

Ethics approval statement

The animal study was reviewed and approved by the Animal Care and Use Committee at the Yellow Sea Fisheries Research Institute, Chinese Academy of Fishery Sciences.

CRediT authorship contribution statement

Tengfei Zhu: Writing – review & editing, Writing – original draft, Visualization, Validation, Supervision, Software, Resources, Project administration, Methodology, Investigation, Funding acquisition, Formal analysis, Data curation, Conceptualization. **Ming Kong:**

Validation, Supervision, Resources, Project administration, Methodology. **Yingying Yu:** Methodology, Investigation, Formal analysis. **Manfred Schartl:** Writing – review & editing, Validation, Methodology. **Deborah Mary Power:** Writing – review & editing, Validation, Methodology. **Chen Li:** Methodology, Investigation, Formal analysis. **Wenxiu Ma:** Investigation, Formal analysis. **Yanxu Sun:** Investigation, Formal analysis. **Shuo Li:** Software, Investigation, Data curation. **Bowen Yue:** Investigation, Formal analysis. **Weijing Li:** Software, Investigation, Data curation. **Changwei Shao:** Writing – review & editing, Validation, Supervision, Resources, Project administration, Methodology, Funding acquisition, Data curation, Conceptualization.

Declaration of Competing Interest

The authors declare that the research was conducted in the absence of any commercial or financial relationships that could be construed as a potential conflict of interest.

Data availability

The data presented in the study are deposited in the NCBI Sequence Read Archive (SRA) repository, accession number PRJNA938023.

Acknowledgements

This work was supported by the National Key Research and Development Program of China (2022YFD2400100), the National Natural Science Foundation of China (32002384), the AoShan Talents Cultivation Program Supported by Qingdao National Laboratory for Marine Science and Technology (2017ASTCP-ES06), the Taishan Scholar Project Fund of Shandong of China, the National Ten-Thousands Talents Special Support Program, the Central Public-interest Scientific Institution Basal Research Fund, CAFS (2020TD19), and the Qingdao Postdoctoral Applied Research Projects.

We thank Dr. Zhihong Gong and Dr. Yadong Chen for their help in cell culture. Thanks are also due to Dr. Yang Liu and Dr. Qianqian Ge for their help in fish rearing, and Dr. Yitao Wang for his assistance in equipment assembly and testing.

Appendix A. Supplementary data

Supplementary data to this article can be found online at https://doi.org/10.1016/j.jconrel.2023.09.027.

References

[1] R. Kalluri, V.S. LeBleu, The biology, function, and biomedical applications of exosomes, Science (80) 367 (2020), https://doi.org/10.1126/science.aau6977.
[2] B. Zhou, K. Xu, X. Zheng, T. Chen, J. Wang, Y. Song, Y. Shao, S. Zheng, Application of exosomes as liquid biopsy in clinical diagnosis, Signal Transduct. Target. Ther. 5 (2020), https://doi.org/10.1038/s41392-020-00258-9.
[3] L. Barile, G. Vassalli, Exosomes: therapy delivery tools and biomarkers of diseases, Pharmacol. Ther. 174 (2017) 63–78, https://doi.org/10.1016/j.pharmthera.2017.02.020.
[4] O.M. Elsharkasy, J.Z. Nordin, D.W. Hagey, O.G. de Jong, R.M. Schiffelers, S.E. L. Andaloussi, P. Vader, Extracellular vesicles as drug delivery systems: why and how? Adv. Drug Deliv. Rev. 159 (2020) 332–343, https://doi.org/10.1016/j.addr.2020.04.004.
[5] B. Yang, Y. Chen, J. Shi, Exosome biochemistry and advanced nanotechnology for next-generation theranostic platforms, Adv. Mater. 31 (2019) 1–33, https://doi.org/10.1002/adma.201802896.
[6] S. Salunkhe, M. Dheeraj, D. Basak, A. Chitkara, Mittal, surface functionalization of exosomes for target-specific delivery and in vivo imaging & tracking: strategies and significance, J. Control. Release 326 (2020) 599–614, https://doi.org/10.1016/j.jconrel.2020.07.042.
[7] G. Jia, Y. Han, Y. An, Y. Ding, C. He, X. Wang, Q. Tang, NRP-1 targeted and cargo-loaded exosomes facilitate simultaneous imaging and therapy of glioma in vitro and in vivo, Biomaterials. 178 (2018) 302–316, https://doi.org/10.1016/j.biomaterials.2018.06.029.
[8] L. Alvarez-Erviti, Y. Seow, H. Yin, C. Betts, S. Lakhal, M.J.A. Wood, Delivery of siRNA to the mouse brain by systemic injection of targeted exosomes, Nat. Biotechnol. 29 (2011) 341–345, https://doi.org/10.1038/nbt.1807.
[9] M. Cully, Exosome-based candidates move into the clinic, Nat. Rev. Drug Discov. 20 (2021) 6–7, https://doi.org/10.1038/d41573-020-00220-y.
[10] Y. Nagahama, T. Chakraborty, B. Paul-Prasanth, K. Ohta, M. Nakamura, Sex determination, gonadal sex differentiation, and plasticity in vertebrate species, Physiol. Rev. 101 (2021) 1237–1308, https://doi.org/10.1152/physrev.00044.2019.
[11] C.K. Matson, D. Zarkower, Sex and the singular DM domain: insights into sexual regulation, evolution and plasticity, Nat. Rev. Genet. 13 (2012) 163–174, https://doi.org/10.1038/nrg3161.
[12] C.A. Smith, P.J. McClive, P.S. Western, K.J. Reed, A.H. Sinclair, Conservation of a sex-determining gene, Nature. 402 (1999) 601–602, https://doi.org/10.1038/45130.
[13] M. Matsuda, Y. Nagahama, A. Shinomiya, T. Sato, C. Matsuda, T. Kobayashi, C. E. Morrey, N. Shibata, S. Asakawa, N. Shimizu, H. Hori, S. Hamaguchi, M. Sakaizumi, DMY is a Y-specific DM-domain gene required for male development in the medaka fish, Nature. 417 (2002) 559–563, https://doi.org/10.1038/nature751.
[14] D.S. Wang, L.Y. Zhou, T. Kobayashi, M. Matsuda, Y. Shibata, F. Sakai, Y. Nagahama, Doublesex- and Mab-3-related transcription factor-1 repression of aromatase transcription, a possible mechanism favoring the male pathway in Tilapia, Endocrinology. 151 (2010) 1331–1340, https://doi.org/10.1210/en.2009-0999.
[15] K.M. Bradley, J.P. Breyer, D.B. Melville, K.W. Broman, E.W. Knapik, J.R. Smith, An SNP-based linkage map for zebrafish reveals sex determination loci, G3 Genes Genomes Genet. 1 (2011) 3–9, https://doi.org/10.1534/g3.111.000190.
[16] S. Yoshimoto, E. Okada, H. Umemoto, K. Tamura, Y. Uno, C. Nishida-Umehara, Y. Matsuda, N. Takamatsu, T. Shiba, M. Ito, A W-linked DM-domain gene, DM-W, participates in primary ovary development in Xenopus laevis, Proc. Natl. Acad. Sci. U. S. A. 105 (2008) 2469–2474, https://doi.org/10.1073/pnas.0712244105.
[17] C.K. Matson, M.W. Murphy, M.D. Griswold, S. Yoshida, V.J. Bardwell, D. Zarkower, The mammalian doublesex homolog DMRT1 is a transcriptional gatekeeper that controls the mitosis versus meiosis decision in male germ cells, Dev. Cell 19 (2010) 612–624, https://doi.org/10.1016/j.devcel.2010.09.010.
[18] C.K. Matson, M.W. Murphy, A.L. Sarver, M.D. Griswold, V.J. Bardwell, D. Zarkower, DMRT1 prevents female reprogramming in the postnatal mammalian testis, Nature. 476 (2011) 101–105, https://doi.org/10.1038/nature10239.
[19] S. Chen, G. Zhang, C. Shao, Q. Huang, G. Liu, P. Zhang, W. Song, N. An, D. Chalopin, J.N. Volff, Y. Hong, Q. Li, Z. Sha, H. Zhou, M. Xie, Q. Yu, Y. Liu, H. Xiang, N. Wang, K. Wu, C. Yang, Q. Zhou, X. Liao, L. Yang, Q. Hu, J. Zhang, L. Meng, L. Jin, Y. Tian, J. Lian, J. Yang, G. Miao, S. Liu, Z. Liang, F. Yan, Y. Li, B. Sun, H. Zhang, J. Zhang, Y. Zhu, M. Du, Y. Zhao, M. Schartl, Q. Tang, J. Wang, Whole-genome sequence of a flatfish provides insights into ZW sex chromosome evolution and adaptation to a benthic lifestyle, Nat. Genet. 46 (2014) 253–260, https://doi.org/10.1038/ng.2890.
[20] C. Shao, Q. Li, S. Chen, P. Zhang, J. Lian, Q. Hu, B. Sun, L. Jin, S. Liu, Z. Wang, H. Zhao, Z. Jin, Z. Liang, Y. Li, Q. Zheng, Y. Zhang, J. Wang, G. Zhang, Epigenetic modification and inheritance in sexual reversal of fish, Genome Res. 24 (2014) 604–615, https://doi.org/10.1101/gr.162172.113.
[21] Z. Cui, Y. Liu, W. Wang, Q. Wang, N. Zhang, F. Lin, N. Wang, C. Shao, Z. Dong, Y. Li, Y. Yang, M. Hu, H. Li, F. Gao, Z. Wei, L. Meng, Y. Liu, M. Wei, Y. Zhu, H. Guo, C.H.K. Cheng, M. Schartl, S. Chen, Genome editing reveals dmrt1 as an essential male sex-determining gene in Chinese tongue sole (Cynoglossus semilaevis), Sci. Rep. 7 (2017) 1–10, https://doi.org/10.1038/srep42213.
[22] L. Tang, F. Huang, W. You, A. Poetsch, R.H. Nóbrega, D.M. Power, T. Zhu, K. Liu, H.Y. Wang, Q. Wang, X. Xu, B. Feng, M. Schartl, C. Shao, ceRNA crosstalk mediated by ncRNAs is a novel regulatory mechanism in fish sex determination and differentiation, Genome Res. 32 (2022) 1502–1515, https://doi.org/10.1101/gr.275962.121.
[23] D. Betel, A. Koppal, P. Agius, C. Sander, C. Leslie, Comprehensive modeling of microRNA targets predicts functional non-conserved and non-canonical sites, Genome Biol. 11 (2010), https://doi.org/10.1186/gb-2010-11-8-r90.
[24] H.Y. Wang, X. Liu, J.Y. Chen, Y. Huang, Y. Lu, F. Tan, Q. Liu, M. Yang, S. Li, X. Zhang, Y. Qin, W. Ma, Y. Yang, L. Meng, K. Liu, Q. Wang, G. Fan, R.H. Nóbrega, S. Liu, F. Piferrer, C. Shao, Single-cell-resolution transcriptome map revealed novel genes involved in testicular germ cell progression and somatic cells specification in Chinese tongue sole with sex reversal, Sci. China Life Sci. (2022) 1–19, https://doi.org/10.1007/s11427-021-2236-4.
[25] R. Evans, M. O'Neill, A. Pritzel, N. Antropova, A.W. Senior, T. Green, A. Žídek, R. Bates, S. Blackwell, J. Yim, Protein complex prediction with AlphaFold-Multimer. BioRxiv 463034 [Preprint], 2021. https://doi.org/10.1101/2021.10.04.463034.
[26] A. Krogh, B. Larsson, G. Von Heijne, E.L.L. Sonnhammer, Predicting transmembrane protein topology with a hidden Markov model: application to complete genomes, J. Mol. Biol. 305 (2001) 567–580, https://doi.org/10.1006/jmbi.2000.4315.
[27] F. Madeira, M. Pearce, A.R.N. Tivey, P. Basutkar, J. Lee, O. Edbali, N. Madhusoodanan, A. Kolesnikov, R. Lopez, Search and sequence analysis tools services from EMBL-EBI in 2022, Nucleic Acids Res. 50 (2022) W276–W279, https://doi.org/10.1093/nar/gkac240.
[28] C. Théry, A. Clayton, S. Amigorena, G. Raposo, Isolation and characterization of exosomes from cell culture supernatants, Curr. Protoc. Cell Biol. 30 (3.22) (2006), 3.22.1–3.22.29.
[29] J. Schindelin, I. Arganda-Carreras, E. Frise, V. Kaynig, M. Longair, T. Pietzsch, S. Preibisch, C. Rueden, S. Saalfeld, B. Schmid, J.Y. Tinevez, D.J. White, V. Hartenstein, K. Eliceiri, P. Tomancak, A. Cardona, Fiji: An open-source platform

for biological-image analysis, Nat. Methods 9 (2012) 676–682, https://doi.org/10.1038/nmeth.2019.
[30] L. Yang, C. SongLin, G. FengTao, M. Liang, H. QiaoMu, S. WenTao, S. ChangWei, L. Weiqun, SCAR-transformation of sex-specific SSR marker and its application in half-smooth tongue sole (Cynoglossus semiliaevis), J. Agric. Biotechnol. 22 (2014) 787–792.
[31] D. Gupta, A.M. Zickler, S. El Andaloussi, Dosing extracellular vesicles, Adv. Drug Deliv. Rev. 178 (2021) 113961, https://doi.org/10.1016/j.addr.2021.113961.
[32] S.S. Hong, M.X. Zhang, M. Zhang, Y. Yu, J. Chen, X.Y. Zhang, C.J. Xu, Follicle-stimulating hormone peptide-conjugated nanoparticles for targeted shRNA delivery lead to effective gro-α silencing and antitumor activity against ovarian cancer, Drug. Deliv. 25 (2018) 576–584, https://doi.org/10.1080/10717544.2018.1440667.
[33] X.Y. Zhang, J. Chen, Y.F. Zheng, X.L. Gao, Y. Kang, J.C. Liu, M.J. Cheng, H. Sun, C. J. Xu, Follicle-stimulating hormone peptide can facilitate paclitaxel nanoparticles to target ovarian carcinoma in vivo, Cancer Res. 69 (2009) 6506–6514, https://doi.org/10.1158/0008-5472.CAN-08-4721.
[34] L. Fan, J. Chen, X. Zhang, Y. Liu, C. Xu, Follicle-stimulating hormone polypeptide modified nanoparticle drug delivery system in the treatment of lymphatic metastasis during ovarian carcinoma therapy, Gynecol. Oncol. 135 (2014) 125–132, https://doi.org/10.1016/j.ygyno.2014.06.030.
[35] C. Théry, K.W. Witwer, E. Aikawa, M.J. Alcaraz, J.D. Anderson, R. Andriantsitohaina, A. Antoniou, T. Arab, F. Archer, G.K. Atkin-Smith, D.C. Ayre, E.K. Zuba-Surma, et al., Minimal information for studies of extracellular vesicles 2018 (MISEV2018): a position statement of the International Society for Extracellular Vesicles and update of the MISEV2014 guidelines, J. Extracell. Vesicles. 7 (2018), https://doi.org/10.1080/20013078.2018.1535750.
[36] N. Cui, G. Hao, Z. Zhao, F. Wang, J. Cao, A. Yang, MicroRNA-224 regulates self-renewal of mouse spermatogonial stem cells via targeting DMRT1, J. Cell. Mol. Med. 20 (2016) 1503–1512, https://doi.org/10.1111/jcmm.12838.
[37] W. Tao, L. Sun, H. Shi, Y. Cheng, D. Jiang, B. Fu, M.A. Conte, W.J. Gammerdinger, T.D. Kocher, D. Wang, Integrated analysis of miRNA and mRNA expression profiles in tilapia gonads at an early stage of sex differentiation, BMC Genomics 17 (2016) 1–13, https://doi.org/10.1186/s12864-016-2636-z.
[38] W. Wang, W. Liu, Q. Liu, B. Li, L. An, R. Hao, J. Zhao, S. Liu, J. Song, Coordinated microRNA and messenger RNA expression profiles for understanding sexual dimorphism of gonads and the potential roles of microRNA in the steroidogenesis pathway in Nile tilapia (Oreochromis niloticus), Theriogenology. 85 (2016) 970–978, https://doi.org/10.1016/j.theriogenology.2015.11.006.
[39] H. Yan, Q. Liu, J. Jiang, X. Shen, L. Zhang, Z. Yuan, Y. Wu, Y. Liu, Identification of sex differentiation-related microRNA and long non-coding RNA in Takifugu rubripes gonads, Sci. Rep. 11 (2021) 1–13, https://doi.org/10.1038/s41598-021-83891-w.
[40] F. De Pascali, A. Tréfier, F. Landomiel, V. Bozon, G. Bruneau, R. Yvinec, A. Poupon, P. Crépieux, E. Reiter, Follicle-stimulating hormone receptor: advances and remaining challenges, Int. Rev. Cell Mol. Biol. 338 (2018) 1–58, https://doi.org/10.1016/bs.ircmb.2018.02.001.
[41] Q.R. Fan, W.A. Hendrickson, Structure of human follicle-stimulating hormone in complex with its receptor, Nature. 433 (2005) 269–277, https://doi.org/10.1038/nature03206.
[42] X. Jiang, H. Liu, X. Chen, P.H. Chen, D. Fischer, V. Sriraman, H.N. Yu, S. Arkinstall, X. He, Structure of follicle-stimulating hormone in complex with the entire ectodomain of its receptor, Proc. Natl. Acad. Sci. U. S. A. 109 (2012) 12491–12496, https://doi.org/10.1073/pnas.1206643109.
[43] J. Jumper, R. Evans, A. Pritzel, T. Green, M. Figurnov, O. Ronneberger, K. Tunyasuvunakool, R. Bates, A. Žídek, A. Potapenko, A. Bridgland, C. Meyer, S.A. A. Kohl, A.J. Ballard, A. Cowie, B. Romera-Paredes, S. Nikolov, R. Jain, J. Adler, T. Back, S. Petersen, D. Reiman, E. Clancy, M. Zielinski, M. Steinegger, M. Pacholska, T. Berghammer, S. Bodenstein, D. Silver, O. Vinyals, A.W. Senior, K. Kavukcuoglu, P. Kohli, D. Hassabis, Highly accurate protein structure prediction with AlphaFold, Nature 596 (2021) 583–589, https://doi.org/10.1038/s41586-021-03819-2.
[44] O.P.B. Wiklander, J.Z. Nordin, A. O'Loughlin, Y. Gustafsson, G. Corso, I. Mäger, P. Vader, Y. Lee, H. Sork, Y. Seow, N. Heldring, L. Alvarez-Erviti, C.I. Edvard Smith, K. Le Blanc, P. Macchiarini, P. Jungebluth, M.J.A. Wood, S. El Andaloussi, Extracellular vesicle in vivo biodistribution is determined by cell source, route of administration and targeting, J. Extracell. Vesicles. 4 (2015) 1–13, https://doi.org/10.3402/jev.v4.26316.
[45] H. Saari, E. Lázaro-Ibáñez, T. Viitala, E. Vuorimaa-Laukkanen, P. Siljander, M. Yliperttula, Microvesicle- and exosome-mediated drug delivery enhances the cytotoxicity of paclitaxel in autologous prostate cancer cells, J. Control. Release 220 (2015) 727–737, https://doi.org/10.1016/j.jconrel.2015.09.031.
[46] Y. Ma, C. Li, Y. Huang, Y. Wang, X. Xia, J.C. Zheng, Exosomes released from neural progenitor cells and induced neural progenitor cells regulate neurogenesis through miR-21a, Cell Commun. Sig. 17 (2019) 1–10, https://doi.org/10.1186/s12964-019-0418-3.
[47] J.P.K. Armstrong, M.N. Holme, M.M. Stevens, Re-engineering extracellular vesicles as smart nanoscale therapeutics, ACS Nano 11 (2017) 69–83, https://doi.org/10.1021/acsnano.6b07607.
[48] G.R. Gunassekaran, S.M. Poongkavithai Vadevoo, M.C. Baek, B. Lee, M1 macrophage exosomes engineered to foster M1 polarization and target the IL-4 receptor inhibit tumor growth by reprogramming tumor-associated macrophages into M1-like macrophages, Biomaterials. 278 (2021) 121137, https://doi.org/10.1016/j.biomaterials.2021.121137.
[49] G.H. Cui, H.D. Guo, H. Li, Y. Zhai, Z. Bin Gong, J. Wu, J.S. Liu, Y.R. Dong, S.X. Hou, J.R. Liu, RVG-modified exosomes derived from mesenchymal stem cells rescue memory deficits by regulating inflammatory responses in a mouse model of Alzheimer's disease, Immun. Ageing 16 (2019) 1–12, https://doi.org/10.1186/s12979-019-0150-2.
[50] A. Vandergriff, K. Huang, D. Shen, S. Hu, M.T. Hensley, T.G. Caranasos, L. Qian, K. Cheng, Targeting regenerative exosomes to myocardial infarction using cardiac homing peptide, Theranostics. 8 (2018) 1869–1878, https://doi.org/10.7150/thno.20524.
[51] B. Mao, T. Bu, D. Mruk, C. Li, F. Sun, C.Y. Cheng, Modulating the blood–testis barrier towards increasing drug delivery, Trends Pharmacol. Sci. 41 (2020) 690–700, https://doi.org/10.1016/j.tips.2020.07.002.
[52] S.I. Ohno, M. Takanashi, K. Sudo, S. Ueda, A. Ishikawa, N. Matsuyama, K. Fujita, T. Mizutani, T. Ohgi, T. Ochiya, N. Gotoh, M. Kuroda, Systemically injected exosomes targeted to EGFR deliver antitumor microrna to breast cancer cells, Mol. Ther. 21 (2013) 185–191, https://doi.org/10.1038/mt.2012.180.
[53] S. El-Andaloussi, Y. Lee, S. Lakhal-Littleton, J. Li, Y. Seow, C. Gardiner, L. Alvarez-Erviti, I.L. Sargent, M.J.A. Wood, Exosome-mediated delivery of siRNA in vitro and in vivo, Nat. Protoc. 7 (2012) 2112–2126, https://doi.org/10.1038/nprot.2012.131.
[54] F. Pi, D.W. Binzel, T.J. Lee, Z. Li, M. Sun, P. Rychahou, H. Li, F. Haque, S. Wang, C. M. Croce, B. Guo, B.M. Evers, P. Guo, Nanoparticle orientation to control RNA loading and ligand display on extracellular vesicles for cancer regression, Nat. Nanotechnol. 13 (2018) 82–89, https://doi.org/10.1038/s41565-017-0012-z.
[55] R.C. de Abreu, C.V. Ramos, C. Becher, M. Lino, C. Jesus, P.A. da Costa Martins, P.A. T. Martins, M.J. Moreno, H. Fernandes, L. Ferreira, Exogenous loading of miRNAs into small extracellular vesicles, J. Extracell. Vesicles. 10 (2021), https://doi.org/10.1002/jev2.12111.
[56] V.R. Harley, M.J. Clarkson, A. Argentaro, The molecular action and regulation of the testis-determining factors, SRY (sex-determining region on the Y chromosome) and Sox9 [Sry-related high-mobility group (HMG) box 9], Endocr. Rev. 24 (2003) 466–487, https://doi.org/10.1210/er.2002-0025.
[57] J.A. Marshall Graves, C.L. Peichel, Are homologies in vertebrate sex determination due to shared ancestry or to limited options? Genome Biol. 11 (2010) https://doi.org/10.1186/gb-2010-11-4-205.
[58] C.E. Bishop, D.J. Whitworth, Y. Qin, A.I. Agoulnik, I.U. Agoulnik, W.R. Harrison, R. R. Behringer, P.A. Overbeek, A transgenic insertion upstream of Sox9 is associated with dominant XX sex reversal in the mouse, Nat. Genet. 26 (2000) 490–494, https://doi.org/10.1038/82652.
[59] V.P.I. Vidal, M.C. Chaboissier, D.G. De Rooij, A. Schedl, Sox9 induces testis development in XX transgenic mice, Nat. Genet. 28 (2001) 216–217, https://doi.org/10.1038/90046.
[60] M. Elzaiat, L. Jouneau, D. Thépot, C. Klopp, A. Allais-Bonnet, C. Cabau, M. André, S. Chaffaux, E.P. Cribiu, E. Pailhoux, M. Pannetier, High-throughput sequencing analyses of XX genital ridges lacking FOXL2 reveal DMRT1 up-regulation before SOX9 expression during the sex-reversal process in goats, Biol. Reprod. 91 (2014) 1–14, https://doi.org/10.1095/biolreprod.114.122796.
[61] S. Kim, V.J. Bardwell, D. Zarkower, Cell type-autonomous and non-autonomous requirements for Dmrt1 in postnatal testis differentiation, Dev. Biol. 307 (2007) 314–327, https://doi.org/10.1016/j.ydbio.2007.04.046.
[62] U. Fahrioglu, M.W. Murphy, D. Zarkower, V.J. Bardwell, mRNA expression analysis and the molecular basis of neonatal testis defects in Dmrt1 mutant mice, Sex. Dev. 1 (2006) 42–58, https://doi.org/10.1159/000096238.
[63] H. Yu, X. Huang, Y. Ma, M. Gao, O. Wang, T. Gao, Y. Shen, X. Liu, Interleukin-8 regulates endothelial permeability by down-regulation of tight junction but not dependent on integrins induced focal adhesions, Int. J. Biol. Sci. 9 (2013) 966–979, https://doi.org/10.7150/ijbs.6996.
[64] D.D. Mruk, C.Y. Cheng, The mammalian blood-testis barrier: its biology and regulation, Endocr. Rev. 36 (2015) 564–591, https://doi.org/10.1210/er.2014-1101.
[65] T. Zhang, J. Oatley, V.J. Bardwell, D. Zarkower, DMRT1 is required for mouse Spermatogonial stem cell maintenance and replenishment, PLoS Genet. 12 (2016) 1–18, https://doi.org/10.1371/journal.pgen.1006293.
[66] R. Nozu, R. Horiguchi, Y. Kobayashi, M. Nakamura, Expression profile of doublesex/male abnormal-3-related transcription factor-1 during gonadal sex change in the protogynous wrasse, Halichoeres trimaculatus, Mol. Reprod. Dev. 82 (2015) 859–866, https://doi.org/10.1002/mrd.22527.
[67] H. Li, Z. Liang, J. Yang, D. Wang, H. Wang, M. Zhu, B. Geng, E.Y. Xu, DAZL is a master translational regulator of murine spermatogenesis, Natl. Sci. Rev. 6 (2019) 455–468, https://doi.org/10.1093/nsr/nwy163.
[68] M.C. Siomi, K. Sato, D. Pezic, A.A. Aravin, PIWI-interacting small RNAs: the vanguard of genome defence, Nat. Rev. Mol. Cell Biol. 12 (2011) 246–258, https://doi.org/10.1038/nrm3089.
[69] B. Gan, S. Chen, H. Liu, J. Min, K. Liu, Structure and function of eTudor domain containing TDRD proteins, Crit. Rev. Biochem. Mol. Biol. 54 (2019) 119–132, https://doi.org/10.1080/10409238.2019.1603199.
[70] B. Wang, H. Wang, H. Song, C. Jin, M. Peng, C. Gao, F. Yang, X. Du, J. Qi, Q. Zhang, J. Cheng, Evolutionary significance and regulated expression of Tdrd family genes in gynogenetic Japanese flounder (Paralichthys olivaceus), Comp. Biochem. Physiol. - Part D Genomics Proteomics. 31 (2019) 100593, https://doi.org/10.1016/j.cbd.2019.05.003.
[71] C.K. Cahoon, R.S. Hawley, Regulating the construction and demolition of the synaptonemal complex, Nat. Struct. Mol. Biol. 23 (2016) 369–377, https://doi.org/10.1038/nsmb.3208.
[72] C.S. Raymond, M.W. Murphy, M.G. O'Sullivan, V.J. Bardwell, D. Zarkower, Dmrt1, a gene related to worm and fly sexual regulators, is required for mammalian testis differentiation, Genes Dev. 14 (2000) 2587–2595, https://doi.org/10.1101/gad.834100.